

Photo-dynamics of photoactivated adenylyl cyclase LiPAC from the spirochete bacterium *Leptonema illini* strain 3055^T

Alfons Penzkofer^{1,*}, Meenakshi Tanwar², Sindhu Kandoth Veetil² and Suneel Kateriya²

¹Fakultät für Physik, Universität Regensburg, Universitätsstraße 31, D-93053 Regensburg, Germany.

²Department of Biochemistry, University of Delhi South Campus, Benito Juarez Road, New Delhi 110021, India.

ABSTRACT

The photoactivated adenylyl cyclase from the spirochete bacterium *Leptonema illini*, abbreviated LiPAC, was synthesized and characterized by absorption and fluorescence spectroscopic methods. LiPAC consists of a BLUF (Blue Light sensor Using Flavin) domain and an adenylyl cyclase homology domain (CHD). Photo-excitation of fully oxidized flavin Fl_{ox} in LiPAC resulted in a typical primary (dark-adapted) BLUF domain photo-cycle dynamics. The quantum efficiency of BLUF domain signaling state formation was determined to be $\phi_s \approx 0.60$. Continued blue-light-excitation of LiPAC in the light-adapted state caused irreversible photo-degradation of non-covalently bound Fl_{ox} to covalently bound fully reduced flavin Fl_{red} with a quantum efficiency of $\phi_D \approx 1.1 \times 10^{-5}$. At 20 °C the time constant of signaling state recovery to the receptor state after excitation light switch-off was $\tau_{rec} \approx 2.6$ s. The protein thermal stability was studied by stepwise sample heating and cooling. An apparent LiPAC melting temperature of 54 °C was determined. Schemes of the primary BLUF domain photo-cycling dynamics and the secondary BLUF domain photo-degradation in the signaling state are presented.

KEYWORDS: Photoactivated adenylyl cyclase LiPAC, optogenetics, spirochete bacterium *Leptonema illini*, BLUF domain photocycle dynamics, flavin photo-degradation in LiPAC, apparent protein melting temperature, quantitative photo-spectroscopic parameter determination

INTRODUCTION

The spirochete bacterium *Leptonema illini* strain 3055^T was first isolated from the urine of a clinically healthy bull [1]. It is also present in kidneys of Indian rats and bandicoots [2]. The bacteriological classification of the *Leptospiraceae* family including *Leptonema illini* is given in [3, 4]. The genome sequence of *Leptonema illini* strain 3055^T was determined recently [5]. The morphology and physiology of *Leptonema illini* strain 3055^T is described in [3, 5]. The *Leptonema illini* strain 3055^T genome consists of 4,522,760 base pairs. The total number of predicted genes is 4277. From them 4230 genes are protein-coding genes. A photoactivated adenylyl cyclase (PAC) gene, named LiPAC, was identified in the genome using homology-based mining of public genome database (NCBI reference sequence: WP_002774553.1).

Photoactivated adenylyl cyclases (PACs) consist of a BLUF (Blue Light sensor Using Flavin) domain and a class III adenylyl cyclase homology domain (CHD) [6]. In PAC proteins blue light excitation of the BLUF domain may activate the catalytic conversion of ATP to cAMP by the CHD

*Corresponding author

alfons.penzkofer@physik.uni-regensburg.de

The paper is dedicated to Prof. Peter Hegemann, Humboldt University, Berlin, Germany, on the occasion of his 60th birthday.

domain [6-18]. Class III adenylyl cyclases are the most wide-spread class of cAMP-generating enzymes [19]. cAMP serves as a second messenger in cells [19, 20]. The light induced second messenger cAMP modulation by PACs in neuronal cells and tissues makes PACs a promising optogenetic tool in cell biology in general and in neuroscience ([7, 8, 9, 12, 17, 18, 21-24] and references therein).

Photoactivated adenylyl cyclases (PACs) that are known to have elevated adenylyl cyclase activity upon blue light irradiation are PAC- α of the eukaryotic unicellular flagellate *Euglena gracilis* [6, 14-18, 23, 24], bPAC of the soil bacterium *Beggiatoa* sp. [7, 8, 11, 25], nPAC (NgPAC1) [9], NgPAC2 [10], and NgPAC3 [12] from the unicellular eukaryotic amoeboid flagellate *Naegleria gruberi*, and NaPAC1 and NaPAC2 from the unicellular eukaryotic amoeboid flagellate *Naegleria australiensis* [26]. In preliminary experiments LiPAC showed light activated adenylyl cyclase activity making it a promising protein for optogenetic applications (investigations will be reported elsewhere).

BLUF domains [27] are seen in many microorganisms either as single sensor domain proteins [28-37] or in multi-domain sensor-actuator proteins as input (sensor) domains [6, 7, 14, 15-18, 38-43]. In the single light sensing BLUF domain proteins the activation of downstream protein modules is thought to occur via intermolecular interaction. In BLUF domain containing multi-domain proteins the activation occurs via intra-molecular interaction. For recent reviews and details on BLUF proteins see [44-47].

Single domain BLUF proteins that have been characterized till now are BlrB from purple bacterium *Rhodobacter sphaeroides* [28, 32, 48] (function unknown), Tll0078 (TePixD) from cyanobacterium *Thermosynechococcus elongates* [33, 34] (function unknown), Slr1694 (SyPixD) from cyanobacterium *Synechocystis* sp. PCC6803 [35-37, 49] (interacts with the response regulator like protein PixE to control phototaxis response [49]), and PapB from purple bacterium *Rhodospseudomonas palustris* [39] (interacts with PapA EAL protein in the blue light-dependent degradation of the cyclic diguanylate).

Known BLUF domain containing proteins are AppA from *Rhodobacter sphaeroides* having a

BLUF and SCHIC domain (SCHIC = sensor containing heme instead of cobalamin) [29, 41, 50-55] (modulates the DNA binding activity of the transcriptional factor PpsR to control the photosynthesis gene expression [50, 55]), BlrP1 from the enteric bacterium *Klebsiellia pneumoniae* having a BLUF and an EAL domain [30, 38, 56] (photo-excitation of the BLUF domain activates the phosphodiesterase activity of the EAL domain causing cyclic dimeric GMP second messenger deactivation by hydrolysis [30, 38]), and YcgF from the enteric bacterium *Escherichia coli* having a BLUF and an EAL domain [57] (interacts with the MerR-like transcriptional factor YcgE to control biofilm formation). In *Euglena gracilis*, a tetramer of PACs (two α -subunits (PAC- α 1 and PAC- α 2) and two β -subunits (PAC- β 1 and PAC- β 2)) act together in photo-avoidance response [6].

Here, the photoactivated cyclase protein LiPAC encoding gene was codon-optimized for expression in *E. coli* and characterized by optical spectroscopic methods for the first time. The absorption and fluorescence behavior of LiPAC in the dark-adapted state (receptor state) and light-adapted state (signaling state) was studied in detail. The flavin loading factor and the flavin composition were determined. The photo-cycling dynamics and the photo-degradation dynamics of LiPAC were analyzed. The thermal stability of LiPAC was characterized by a stepwise sample heating and cooling cycle. Thereby the apparent protein melting temperature was determined. The high protein melting temperature of 54 °C allows stable LiPAC handling at room temperature. Different from other PACs, part of the flavin in LiPAC was found to be fully reduced and covalently bound to the protein. The primary photo-cycle dynamics (starting from receptor state) of the BLUF domain in LiPAC was studied quantitatively and a detailed description of the photo-cycle mechanism with new insights is developed. The secondary photo-cycle dynamics (photo-excitation from the signaling state) was investigated carefully. In doing so, besides efficient photo-induced electron transfer and charge recombination, low-efficient photo-degradation of flavin in LiPAC to covalently bound reduced flavin was discovered. A scheme of the secondary photo-cycle dynamics and photo-degradation is presented.

MATERIALS AND METHODS

Sample preparation

The gene for the photoactivated adenylyl cyclase LiPAC was synthesized with codon usage optimized for expression in *E. coli*. The PAC gene was cloned in frame after N-terminus His tag into pASK vector (IBA, Germany) under Bam HI and Xho I restriction sites. Standard PCR-based molecular biology methods were adapted for cloning of LiPAC gene into expression vector. All DNA constructs were sequenced with automated DNA sequencing methods for confirmation.

The LiPAC pASK construct was transformed into *Escherichia coli* expression strain B1-21DE3 λ . The cells were grown to an optical density of OD_{600 nm} = 0.6 in terrific broth medium (TBM) with appropriate antibiotics at 37 °C, and thereafter recombinant protein expression was induced with anhydrotetracycline (200 μ g/liter) for 48 h at 16 °C. The cells were harvested by centrifugation at 6000 rpm for 10 min, the cell pellet was re-suspended in 1X PBS buffer (pH 7.4) and the re-suspended cells were lysed by sonication. To obtain a soluble fraction containing the protein of interest, lysed cells were centrifuged at 13,000 rpm for 55 min at 4 °C. The LiPAC protein was purified from the soluble fraction with immobilized metal affinity chromatography (IMAC) using Co²⁺ metal ion resins (Clontech, Laboratories Inc. USA) according to supplier's instructions. The LiPAC protein was eluted in PBS buffer containing 500 mM imidazole. The eluted protein was then dialyzed against phosphate buffer pH 7.5 (10 mM NaH₂PO₄/Na₂HPO₄, 10 mM NaCl). All the protein preparation works were carried out under safe light/dark at ambient temperature.

Spectroscopic characterization

The LiPAC protein in pH 7.5 phosphate buffer (10 mM NaH₂PO₄/Na₂HPO₄, 10 mM NaCl) was stored at -80 °C (for experiments presented in Fig. 4 and Fig. 5) or at -25 °C (for experiments presented in Figs. 2, 3 and 6). Before usage the LiPAC protein was thawed and then kept in the dark at 4 °C. All experiments (absorption, fluorescence, and photo-cycle measurements) were carried out at room temperature (21 \pm 1 °C) except the thermal stability investigations (Fig. 5) and the temperature dependent signaling state

recovery time measurements (Fig. 6c). The LiPAC solutions were investigated in fused silica ultra micro cells (inner size 1.5 \times 3 \times 5 mm³) under aerobic conditions.

The transmission measurements were carried out with a spectrophotometer (Cary 50 from Varian). Attenuation coefficient spectra $\alpha(\lambda)$ were calculated from the measured transmission spectra $T(\lambda)$ using the relation $\alpha(\lambda) = -\ln[T(\lambda)]/\ell$, where ℓ is the sample length. For fluorescence spectroscopic measurements a spectrofluorimeter (Cary Eclipse from Varian) was used. Fluorescence quantum distributions $E_F(\lambda)$ were determined from fluorescence emission spectra measurements at fixed excitation wavelengths [58-60]. The dye rhodamine 6G in methanol was used as a calibration reference standard (its fluorescence quantum yield is $\phi_F = 0.94$ [61]). Fluorescence excitation quantum distributions $E_{ex}(\lambda)$ were determined from fluorescence excitation spectra measurements at fixed fluorescence detection wavelengths [62]. The flavin loading factor and the flavin composition were determined from absorption and fluorescence analysis after protein denaturing (heating up to 81 °C keeping this temperature for 4 min, then cooling down to 35 °C, after that centrifugation at 4 °C with 4400 rpm for 25 min). For photo-cycling and photo-degradation investigations, LiPAC samples were brought to the signaling state (light-adapted state) by exposure with a light emitting diode (LED 455 nm from Thorlabs). The temperature dependence of the signaling state recovery to the receptor state (dark-adapted state) was studied by photo-cycle measurements at fixed temperatures in the range from 4 °C to 20 °C. Fluorescence lifetime measurements were performed using a mode-locked titanium sapphire laser (Hurricane from Spectra-Physics) for sample excitation and a micro-channel-plate photomultiplier (Hamamatsu type R1564U-01) or an ultrafast streak-camera (type C1587 temporal disperser with M1952 high-speed streak unit from Hamamatsu) for fluorescence signal detection. The thermal protein stability was studied by stepwise sample heating up to 84.5 °C and cooling down to 4 °C. The apparent protein melting temperature of LiPAC was determined by accompanying absorption spectra measurements [10, 63].

RESULTS

Homology analysis

Multiple sequence alignment [64-66] of LiPAC from *Leptonema illini*, bPAC from *Beggiatoa* sp. [8], NgPAC1 [9] and NgPAC2 [10] from *Naegleria gruberi* is displayed in Fig. 1. It shows the presence of conserved residues for flavin binding in the BLUF domain and of catalytically important residues for the cyclase domain in LiPAC. Details are given in the caption of Fig. 1.

Spectroscopic characterization of unexposed LiPAC

Absorption spectra

The attenuation coefficient spectrum $\alpha(\lambda)$ of an investigated fresh LiPAC sample in the dark after centrifugation (4400 rpm for 15 min) is shown by the thick solid curve in Fig. 2. It is composed of an absorption contribution $\alpha_{\text{abs}}(\lambda)$ and a scattering contribution $\alpha_{\text{sca}}(\lambda)$, i.e. $\alpha(\lambda) = \alpha_{\text{abs}}(\lambda) + \alpha_{\text{sca}}(\lambda)$. The approximate scattering contribution is shown by the triple-dotted curve (empirical power law fit [67-69] $\alpha_{\text{sca}}(\lambda) = \alpha_{\text{sca}}(\lambda_0)(\lambda_0/\lambda)^\gamma$ with $\lambda_0 = 800$ nm, $\alpha_{\text{sca}}(\lambda_0) = 0.044$ cm⁻¹, and $\gamma = 1.9$, γ depends on the scattering particle size). The absorption contribution is shown by the thin solid curve. The dashed curve shows the absorption coefficient spectrum of the LiPAC sample after thermal denaturing. For comparison, the absorption coefficient spectrum of FMN in aqueous solution at pH 7 adjusted at 446 nm to the absorption coefficient of the fresh LiPAC sample is included (see dash-dotted curve).

The absorption coefficient spectrum $\alpha_{\text{abs,LiPAC}}(\lambda)$ (thin solid curve) indicates several features: In the wavelength range from 520 nm to 640 nm the absorption spectrum is caused by semi-reduced flavin Fl_{sq} (FIH⁻). In the wavelength range from 310 nm to 520 nm $\alpha_{\text{abs,LiPAC}}(\lambda)$ is dominated by fully oxidized flavin Fl_{ox} absorption (flavin quinone). Increased absorption in the range from 310 nm to 400 nm indicates the presence of fully reduced flavin Fl_{red} (flavin hydroquinone, for the various redox states of flavin see [70]). Below 310 nm Fl_{ox}, Fl_{red}, Trp and Tyr determine the LiPAC absorption.

The flavin S₀-S₁ absorption band of fresh dark-adapted LiPAC exhibits a vibronic structure indicating an ordered arrangement in the BLUF

domain. Denaturation of LiPAC changed the absorption coefficient spectrum from the thin solid curve to the dashed curve. The Fl_{sq} absorption contribution is lost by denaturation (Fl_{sq} release to the solvent and re-oxidation to Fl_{ox}), the Fl_{ox} absorption tail is approximately 13 nm red-shifted and the spectral vibronic fine-structure is lost (Fl_{ox} release to the solvent). Unexpectedly, the Fl_{red} absorption in the range from 310 nm to 380 nm remained unchanged (no conversion of Fl_{red} to Fl_{ox} which would occur in the case of Fl_{red} release from the protein to the buffer solution in the process of denaturation [71]). This indicates that Fl_{red} is covalently bound to the LiPAC apo-protein hindering re-oxidation (see below).

For the investigated fresh LiPAC sample (thin solid curve in Fig. 2), the number density of flavin semiquinone is estimated to be $N_{\text{FIH}^-} \approx \alpha_{\text{abs,LiPAC}}(580 \text{ nm}) / \sigma_{\text{FNMH}^-}(580 \text{ nm}) \approx 4.7 \times 10^{14}$ cm⁻³ using $\sigma_{\text{FNMH}^-}(580 \text{ nm}) = 1.82 \times 10^{-17}$ cm² (from [72]). The number density of flavin quinone is determined to be $N_{\text{Fl}_{\text{ox}}} = \alpha_{\text{abs,LiPAC,denatured}}(445 \text{ nm}) / \sigma_{\text{FMN}}(445 \text{ nm}) = 2.9 \times 10^{16}$ cm⁻³ using $\sigma_{\text{FMN}}(445 \text{ nm}) = 4.6 \times 10^{-17}$ cm² (from [73]). The number density of flavin hydroquinone is estimated from the LiPAC absorption at 335 nm where the absorption cross-section of FMN and FNMH₂ or FNMH⁻ are about the same [71]. The relation $N_{\text{Fl}_{\text{red}}} = \alpha_{\text{abs,LiPAC}}(335 \text{ nm}) / \sigma_{\text{FMN}}(335 \text{ nm}) - N_{\text{Fl}_{\text{ox}}}$ gives $N_{\text{red}} = 1.14 \times 10^{16}$ cm² using $\sigma_{\text{FMN}}(335 \text{ nm}) = 1.99 \times 10^{-17}$ cm². The LiPAC apo-protein number density is calculated at 270 nm where Trp (number per protein $n_{\text{Trp}} = 1$, absorption cross-section $\sigma_{\text{Trp}} = 1.994 \times 10^{-17}$ cm² [74]), Tyr ($n_{\text{Tyr}} = 8$, $\sigma_{\text{Tyr}} = 4.672 \times 10^{-18}$ cm² [74]), Fl_{ox} ($\sigma_{\text{FMN}} = 1.326 \times 10^{-16}$ cm² [73]) and Fl_{red} ($\sigma_{\text{FNMH}^-} \approx 3.5 \times 10^{-17}$ cm² [71]).

The result is $N_{\text{apo-protein}} \approx 8.27 \times 10^{16}$ cm⁻³. The flavin loading factor is $\kappa_{\text{Fl,load}} = (N_{\text{Fl}_{\text{ox}}} + N_{\text{Fl}_{\text{red}}} + N_{\text{Fl}_{\text{sq}}}) / N_{\text{apo-protein}} \approx 0.49$.

Fluorescence behavior

Fluorescence quantum distributions $E_{\text{F}}(\lambda)$ of fresh dark-adapted LiPAC are shown in the top part of Fig. 3. The solid curve belongs to fluorescence excitation at $\lambda_{\text{F,exc}} = 450$ nm where only the flavin cofactor is excited. The corresponding fluorescence quantum yield is $\phi_{\text{F}} = \int E_{\text{F}}(\lambda) d\lambda = 0.0092 \pm 0.001$.

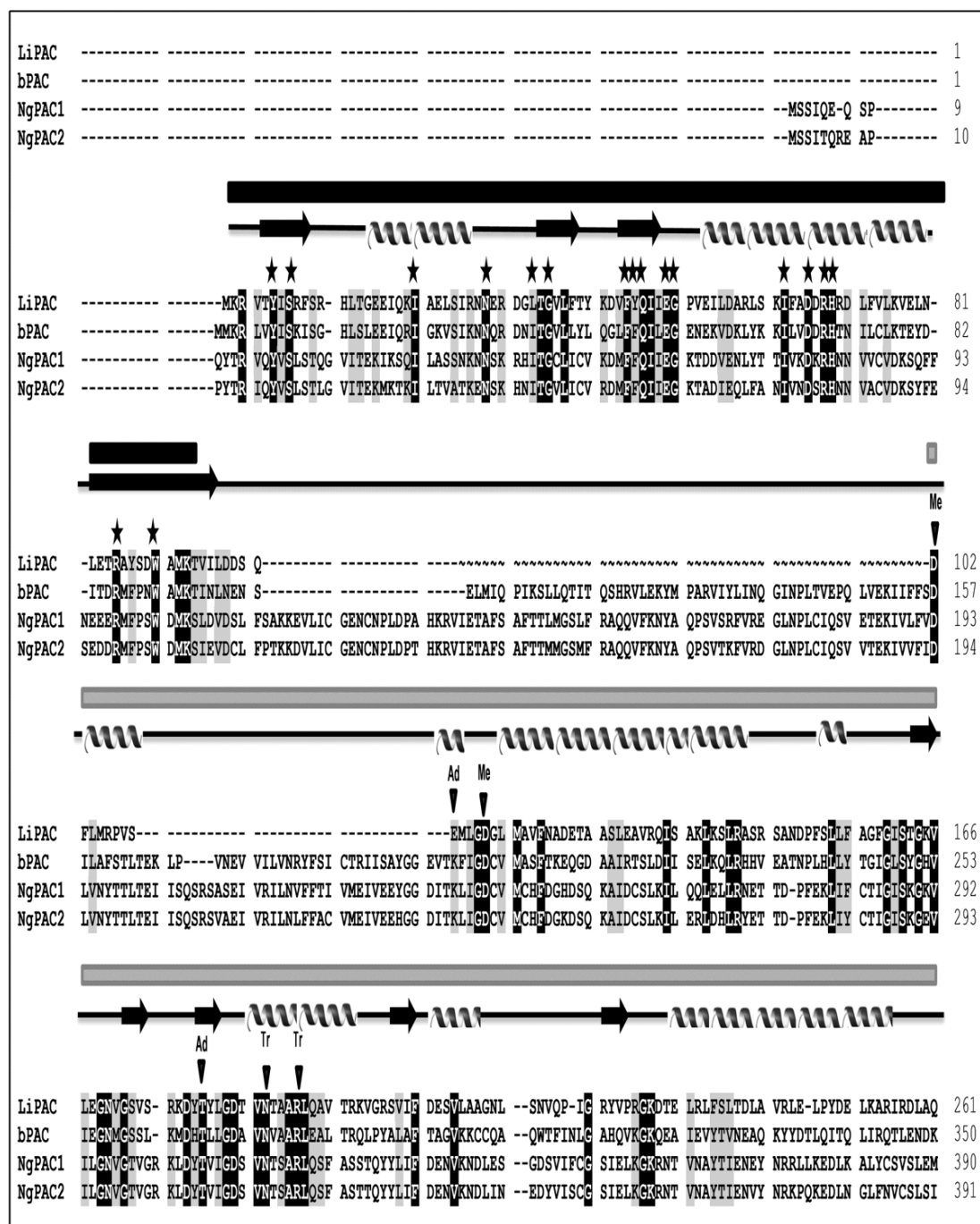


Fig. 1. Multiple sequence alignment of LiPAC from *Leptonema illini* with bPAC from *Beggiatoa* sp. [8], NgPAC1 from *Naegleria gruberi* [9] and NgPAC2 from *Naegleria gruberi* [10] protein sequences. Identical amino acid residues are shown in white on black background and similar residues (greater than 80% similarity) are displayed in black on grey background. The residues of BLUF domain and cyclase domain are designated with black and grey solid bars, respectively. BLUF domain conserved residues are indicated with star. Catalytic conserved residues of cyclase domain: metal binding residue Asp (Me), essential adenine/guanine binding residue Lys or Thr or Glu, and transition state stabilizing residue Asn and Arg are presented with black arrow heads. GOR IV program was used [97] to predict the secondary structure of LiPAC. It suggests that the protein consists of both α -helices and β -sheets. α -helices, β -sheets and random coils are represented with helical cartoons, arrows and lines, respectively.

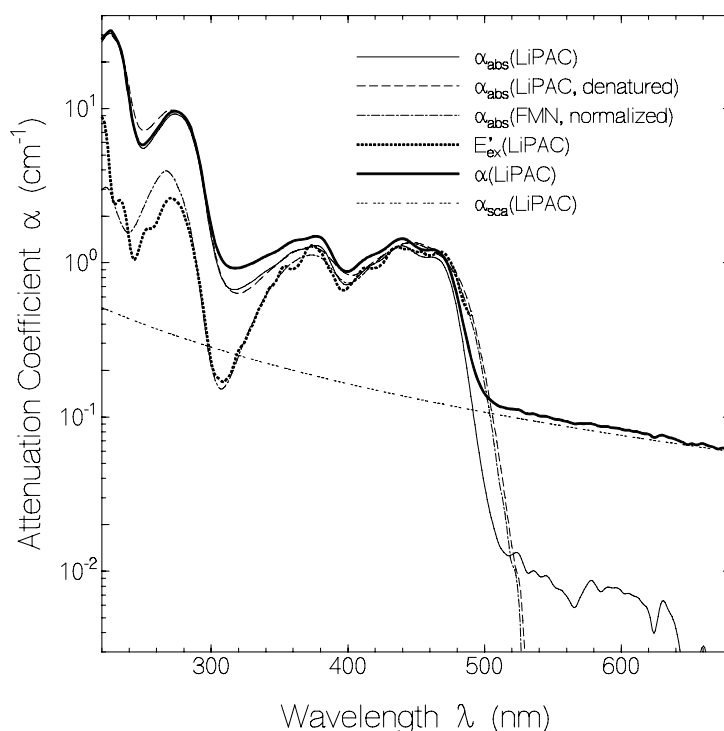


Fig. 2. Absorption behavior of unexposed LiPAC sample in pH 7.5 phosphate buffer. Thick solid curve: attenuation coefficient spectrum $\alpha(\lambda) = \alpha_{\text{abs}}(\lambda) + \alpha_{\text{sca}}(\lambda)$ measured after centrifugation (4400 rpm for 15 min). Triple-dotted curve: approximate scattering contribution $\alpha_{\text{sca}}(\lambda)$. Thin solid curve: absorption coefficient spectrum contribution $\alpha_{\text{abs}}(\lambda)$. Dashed curve: absorption coefficient spectrum of used LiPAC sample after denaturation. Dash-dotted curve: absorption coefficient spectrum of FMN in aqueous solution at pH 7 normalized to $\alpha_{\text{abs,LiPAC}}(446 \text{ nm})$. Dotted curve: fluorescence excitation quantum distribution $E'_{\text{ex}}(\lambda)$ normalized to $\alpha_{\text{abs,LiPAC}}(446 \text{ nm})$ for $\lambda_{\text{F,det}} = 510 \text{ nm}$.

The fluorescence spectrum comprises non-covalently bound flavin Fl_{ox} emission (short wavelength part) and free (released, or improper bound) flavin Fl_{ox} emission (long-wavelength part, Fl_{red} and Fl_{sq} are practically non-fluorescent [70]). The dashed curve was obtained by fluorescence excitation at $\lambda_{\text{F,exc}} = 350 \text{ nm}$. The fluorescence quantum yield is $\phi_{\text{F}} = 0.009 \pm 0.001$. The dotted curve was obtained by fluorescence excitation at $\lambda_{\text{F,exc}} = 270 \text{ nm}$ where Tyr, Trp, and flavin are absorbing. Its fluorescence quantum yield is $\phi_{\text{F}} = 0.0373 \pm 0.003$. The dominant part peaking at 333 nm is due to Trp emission, and the long-wavelength part ($\lambda > 470 \text{ nm}$) is due to flavin emission. The Tyr emission expected to peak at $\approx 305 \text{ nm}$ is strongly quenched (only weak shoulder is seen, spectrum is hidden in dominant Trp spectrum) due to efficient Förster-type [58] Tyr to Trp energy transfer (see supporting information to [75]). The fluorescence quantum

yield contribution from Trp is $\phi_{\text{F,Trp}} \approx 0.0349$ and the fluorescence quantum yield contribution from flavin is $\phi_{\text{F,Fl}} \approx 0.0024$.

A fluorescence excitation quantum distribution of LiPAC is included in Fig. 2 (thick dotted curve). The fluorescence signal was detected at $\lambda_{\text{F,det}} = 510 \text{ nm}$. The presented curve is adjusted to the absorption coefficient $\alpha_{\text{abs}}(\text{LiPAC})$ at $\lambda = 446 \text{ nm}$, i.e. $E'_{\text{ex}}(\lambda) = [E_{\text{ex}}(\lambda) / E_{\text{ex}}(446 \text{ nm})] \alpha_{\text{abs,LiPAC}}(446 \text{ nm})$ is displayed. The curve is determined by fluorescence contributions from free (or improper bound) flavin (giving long-wavelength peak at 469 nm) and non-covalently bound flavin. The shape of $E'_{\text{ex}}(\lambda)$ resembles the combined shape of the absorption spectra of free and non-covalently bound flavin. The deviation of $E'_{\text{ex}}(\lambda)$ from $\alpha_{\text{abs}}(\lambda)$ of FMN below 300 nm is thought to be due to additional higher excited-state to ground-state relaxation paths of flavin besides the higher

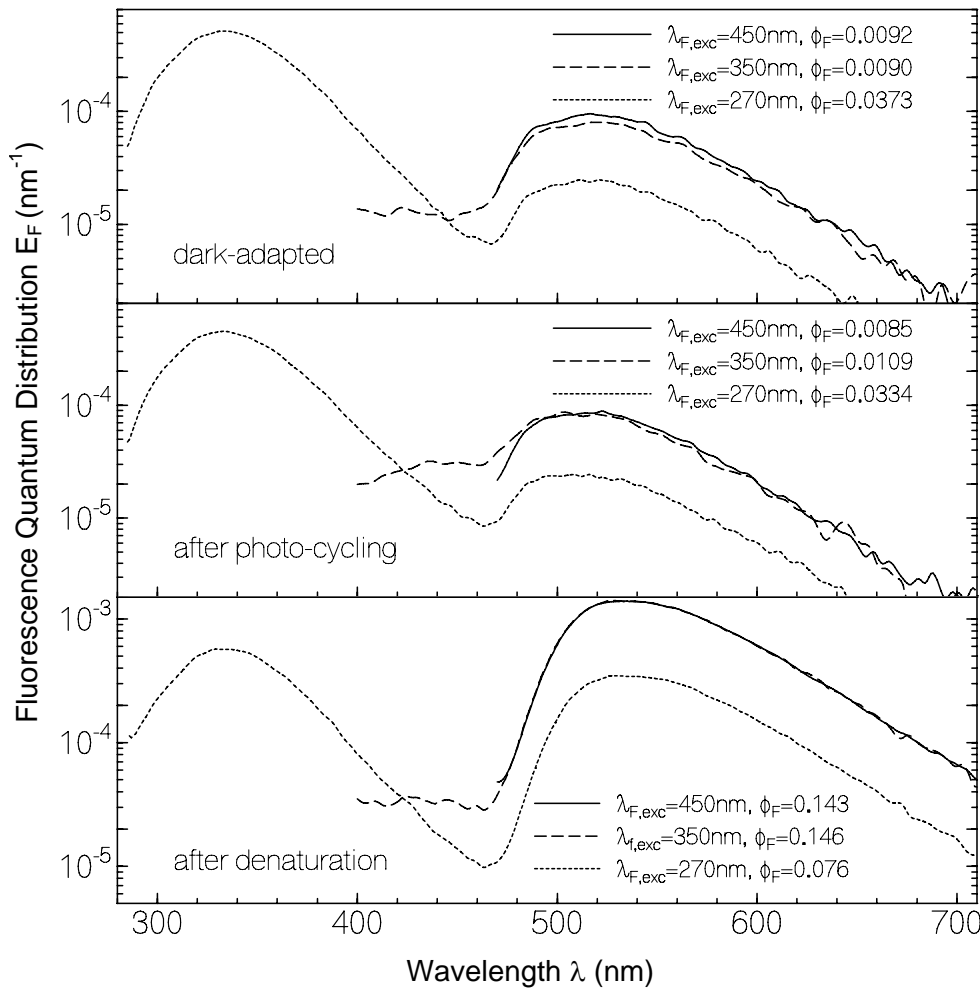


Fig. 3. Top part: Fluorescence quantum distributions $E_F(\lambda)$ of fresh dark-adapted LiPAC in pH 7.5 phosphate buffer for fluorescence excitation wavelengths $\lambda_{F,exc} = 450$ nm (solid curve), 350 nm (dashed curve), and $\lambda_{F,exc} = 270$ nm (dotted curve). Middle part: Fluorescence quantum distributions $E_F(\lambda)$ of sample after photo-cycling experiments (exposed energy density $W_{exp} = 18 \text{ J cm}^{-2}$ at $\lambda_{exc} = 455$ nm). Solid curve: $\lambda_{F,exc} = 450$ nm. Dashed curve: $\lambda_{F,exc} = 350$ nm. Dotted curve: $\lambda_{F,exc} = 270$ nm. Bottom part: Fluorescence quantum distributions $E_F(\lambda)$ of LiPAC sample after denaturation. Solid curve: $\lambda_{F,exc} = 450$ nm. Dashed curve: $\lambda_{F,exc} = 350$ nm. Dotted curve: $\lambda_{F,exc} = 270$ nm. The fluorescence quantum yields ϕ_F are listed in the sub-figures.

excited state to S_1 -state, and S_1 -state to ground-state relaxation path (violation of Vavilov-Kasha rule of wavelength independent fluorescence emission [76, 77]).

Results of fluorescence lifetime measurements are shown in Fig. 4. The fluorescence was excited with 3 ps laser pulses at 400 nm. The solid trace shown in the top part of Fig. 4 was detected with a micro-channel plate photomultiplier (time resolution ≈ 500 ps). The signal decay fits to a bi-exponential function $S_F(t)/S_{F,max} = x_1 \exp(-t/\tau_1) + x_2 \exp(-t/\tau_2)$

with $x_1 = 0.9053$, $\tau_1 = 500$ ps, $x_2 = 0.0947$, and $\tau_2 = 5$ ns (curve not shown). The fast decaying part belongs to non-covalently bound flavin and the slow decaying part belongs to free (or improper bound) flavin. The dotted curve depicts the free (or improper bound) flavin fluorescence contribution. The ratio of the time-integrated free (or improper bound) flavin signal to the total time-integrated flavin signal is $\kappa_{free} = \int S_{F,Fl,free} dt / \int S_{F,Fl} dt = 0.37$. The fraction of free (or improper bound) flavin x_{free} is estimated

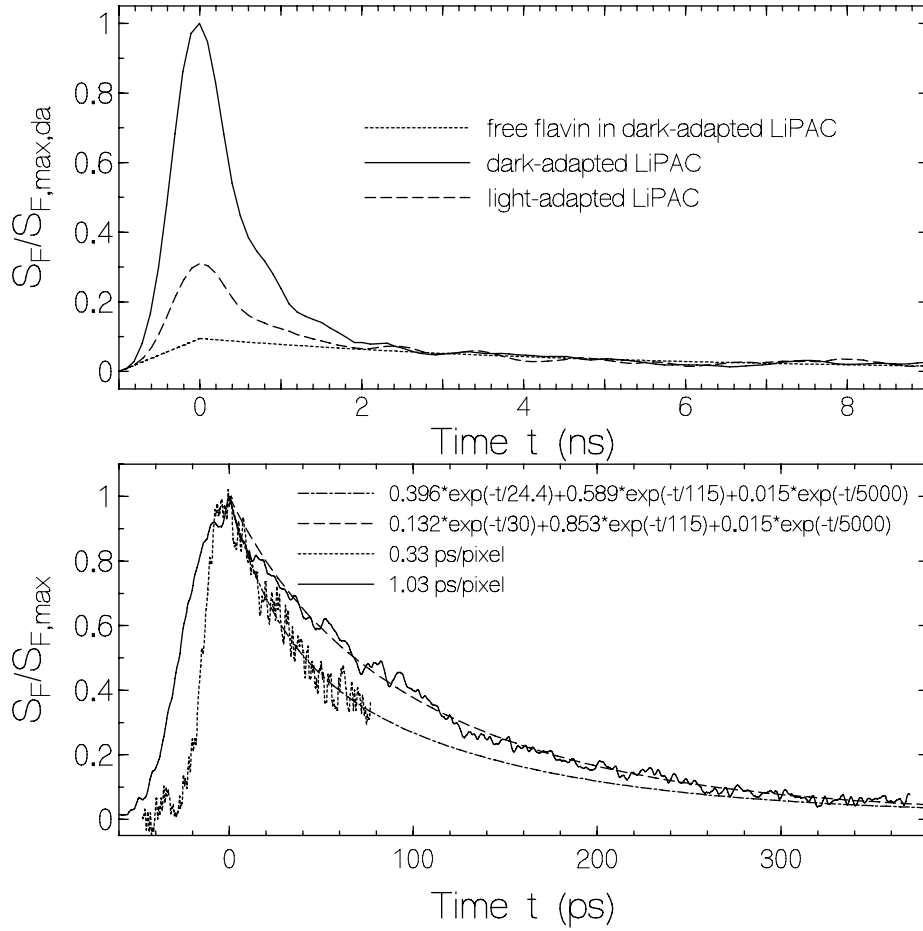


Fig. 4. Temporal fluorescence traces for LiPAC in pH 7.5 phosphate buffer. Sample excitation with 3 ps pulses at 400 nm. Top part: Fluorescence detection with micro-channel-plate photomultiplier (time resolution ≈ 500 ps). Solid curve: dark-adapted sample. Dashed curve: light-adapted sample ($\lambda_{\text{exc}} = 455$ nm, $I_{\text{exc}} = 31.8$ mW cm $^{-2}$, $t_{\text{exc}} = 17$ s). Dotted curve: signal contribution from free (released or improper bound) flavin. Bottom part: Fluorescence detection with ultrafast streak camera using streak speeds of 1.03 ps/pixel (solid curve, time resolution ≈ 30 ps), and of 0.33 ps/pixel (dotted curve, time resolution ≈ 10 ps). Dashed curve is triple-exponential fit to solid experimental curve. Dash-dotted curve is triple-exponential fit to dotted experimental curve.

using the relation $x_{\text{free}} \approx \kappa_{\text{free}} \phi_{F,Fl} / \phi_{F,FMN} \approx 0.015$

with $\phi_{F,FMN} = 0.23$ [73] and $\phi_{F,Fl} = 0.0092$. The fluorescence quantum yield of non-covalently bound flavin is $\phi_{F,Fl,b,da} = \phi_{F,Fl} (1 - \kappa_{\text{free}}) / (1 - x_{\text{free}}) \approx 5.9 \times 10^{-3}$.

The lower part of Fig. 4 shows two fluorescence traces for dark-adapted LiPAC detected with our streak camera system. The solid trace was measured with full-frame streak duration of 1 ns (streak speed 1.03 ps/pixel, time resolution ≈ 30 ps) and the dotted trace was measured with full-frame streak duration of 300 ps (streak speed 0.33 ps/pixel, time resolution ≈ 10 ps). Both traces agree

to a three-component fluorescence decay with lifetimes $\tau_{F,Fl,b,f,da} = 24.4 \pm 2$ ps (amplitude $x_{Fl,da,f} \approx 0.396$), $\tau_{F,Fl,b,sl,da} = 115 \pm 5$ ps (amplitude $x_{Fl,da,sl} \approx 0.589$) of non-covalently bound flavin, and $\tau_{Fl,free} = 5$ ns (amplitude $x_{\text{free}} \approx 0.015$) of free (released or improper bound) flavin. The average fluorescence lifetime of non-covalently bound flavin in dark-adapted LiPAC may be determined by the relation $\bar{\tau}_{F,Fl,b,da} = (x_{b,f} \tau_{F,Fl,b,f,da} + x_{b,sl} \tau_{F,Fl,b,sl,da})$ with $x_{b,f} = x_{Fl,da,f} / (x_{Fl,da,f} + x_{Fl,da,sl}) = 0.402$ and $x_{b,sl} = x_{Fl,da,sl} / (x_{Fl,da,f} + x_{Fl,da,sl}) = 0.598$ giving $\bar{\tau}_{F,Fl,b,da} = 79 \pm 4$ ps.

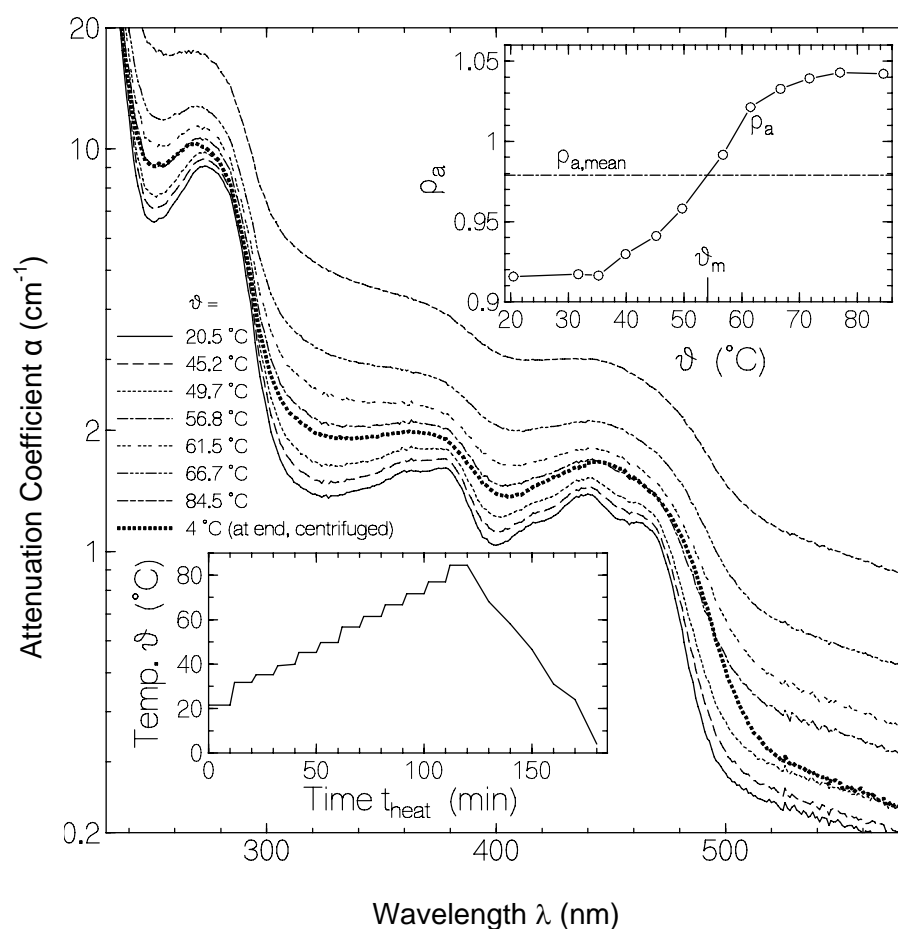


Fig. 5. LiPAC sample heating behavior. Main figure: Attenuation coefficient spectra $\alpha(\lambda)$ development during stepwise sample heating and at end of sample cooling. Sample temperatures belonging to the presented curves are listed in the legend. Lower left inset: Applied temporal heating profile. Upper right inset: Solid curve: Attenuation coefficient ratio $\rho_a = 2\alpha(454 \text{ nm})/[\alpha(440 \text{ nm}) + \alpha(462 \text{ nm})]$ is plotted versus sample temperature. Dash-dotted curve: Mean attenuation coefficient ratio $\rho_{a,mean} = (\rho_{a,min} + \rho_{a,max})/2$. Apparent protein melting temperature ϑ_m is determined by the crossing point of $\rho_a(\vartheta)$ and $\rho_{a,mean}$.

Thermal investigations

One LiPAC sample (sample A) was heated up from room temperature to 81 °C within 15 min, kept at 81 °C for 4 min, cooled down to 35 °C within 8 min, and then centrifuged at 4 °C for 25 min at 4400 rpm. This sample was used for the protein denaturation studies described above (Fig. 2) and for the determination of the flavin composition by fluorescence quantum yield measurement of denatured sample (see below).

A second LiPAC sample (sample B) was used for determination of the apparent LiPAC protein melting temperature. This sample was, after

thawing, kept in the dark at 4 °C for 10 days before usage. It was stepwise heated up to 84.5 °C, and then cooled down. The sample absorption spectrum was measured periodically. The apparent LiPAC protein melting temperature was derived from the loss of the vibronic structure of the S_0 - S_1 absorption band of the flavin cofactor in LiPAC with sample heating [63].

The heating-cooling temperature profile applied to the LiPAC sample B for the apparent melting temperature determination is displayed in the lower inset of Fig. 5. The main part of Fig. 5 shows the attenuation coefficient spectra of LiPAC measured at selected temperatures during

the sample heating up and at the end of the sample cooling down. The temperatures belonging to the curves are given in the legend. With rising temperature, the light scattering increased (see increasing attenuation coefficient spectra) and the spectral structure of the S_0 - S_1 absorption band of flavin (wavelength region from 400 nm to 500 nm) smoothed out. The increase of light scattering may be due to thermal stirring up of protein debris sediment and clustering of denatured (unfolded) protein. The upper right inset of Fig. 5 shows the loss of the dip in the attenuation spectrum at $\lambda = 454$ nm with rising temperature due to protein denaturing (protein unfolding). The ratio $\rho_a(\vartheta) = 2\alpha(454 \text{ nm}, \vartheta) / [\alpha(440 \text{ nm}, \vartheta) + \alpha(462 \text{ nm}, \vartheta)]$ is displayed (line-connected circles). The dash-dotted line is given by $\rho_{a,mean} = [\rho_a(20.5 \text{ }^\circ\text{C}) + \rho_a(84.5 \text{ }^\circ\text{C})]/2$. The apparent LiPAC melting temperature is defined by ϑ_m where $\rho_a(\vartheta_m) = \rho_{a,mean}$. A value of $\vartheta_m = 54 \pm 2 \text{ }^\circ\text{C}$ is determined.

The light attenuation coefficient spectra of LiPAC sample B before heating (solid curve) and after cooling down to 4 $^\circ\text{C}$ and centrifuging at 3500 rpm for 5 min (thick dotted curve) are compared in the main part of Fig. 5. The denatured LiPAC scattered stronger than the native protein due to protein unfolding (random coil formation) and clustering [63]. The vibronic structure of the S_0 - S_1 absorption band and the S_0 - S_2 absorption band are lost and the rise of the long-wavelength absorption tail is less steep indicating release of the flavin

from the BLUF domain in the process of irreversible protein unfolding (protein denaturing).

The fluorescence quantum distribution behavior of the denatured LiPAC sample A is shown in the bottom part of Fig. 3. The dotted curve belongs to fluorescence excitation at $\lambda_{F,exc} = 270$ nm. The total fluorescence quantum yield is $\phi_F(270 \text{ nm}) = 0.076 \pm 0.01$. The band peaking at 332 nm belongs to Trp emission (fluorescence contribution ≈ 0.040 , absorption contribution of Trp and Tyr is approximately 0.53 giving absorption based fluorescence quantum yield of $\phi_{F,Trp} \approx 0.0755$) and the band peaking at 533 nm belongs to free flavin (fluorescence contribution 0.036, absorption contribution ≈ 0.42 giving absorption based fluorescence quantum yield of $\phi_{F,Fl} \approx 0.086$). The dashed curve in the bottom part of Fig. 3 belongs to fluorescence excitation at $\lambda_{F,exc} = 350$ nm. The fluorescence quantum yield is $\phi_F = 0.146 \pm 0.02$. It is determined by free Fl_{ox} emission (flavin released from protein in the denaturation process). The solid curve in the bottom part of Fig. 3 belongs to fluorescence excitation at $\lambda_{F,exc} = 450$ nm. The obtained fluorescence quantum yield is $\phi_{F,Fl,denatured} = 0.143 \pm 0.02$. This fluorescence quantum yield of the denatured LiPAC is higher than that of FAD ($\phi_{FAD} = 0.033$ [78]) and lower than that of FMN ($\phi_{FMN} = 0.23$ [73]) or riboflavin ($\phi_{RF} = 0.26$ [79]) in neutral aqueous solution. It is known that BLUF domains accept FAD, FMN and riboflavin (RF) as cofactor [80]. The flavin quantum yield is given by

$$\begin{aligned} \phi_{F,Fl,denatured} &= x_{FMN}\phi_{FMN} + x_{RF}\phi_{RF} + x_{FAD}\phi_{FAD} \approx x_{FMN,RF}\phi_{FMN} + x_{FAD}\phi_{FAD} \\ &= x_{FMN,RF}\phi_{FMN} + (1 - x_{FMN,RF})\phi_{FAD} \end{aligned} \quad (1)$$

where x_{FMN} , x_{RF} , and x_{FAD} are the mole-fractions of FMN, RF, and FAD, respectively. $x_{FMN,RF} = x_{FMN} + x_{RF}$ is the mole-fraction of FMN and RF together. From the experimental result of $\phi_{F,Fl,denatured}$ only mole-fractions $x_{FMN,RF}$ and $x_{FAD} = 1 - x_{FMN,RF}$ can be estimated. The result is $x_{FMN,RF} = 0.56 \pm 0.1$ and $x_{FAD} \approx 0.44 \pm 0.1$. The fraction $x_{FMN,RF}$ cannot be separated into the fraction x_{FMN} and x_{RF} since the fluorescence quantum yields of FMN and RF are too similar.

Spectroscopic characterization of light exposed LiPAC

Absorption photo-cycling

The photo-cyclic absorption behavior of LiPAC presented in Figs. 6a and 6b was studied at room temperature. The sample solution in our small-volume $1.5 \times 3 \times 5 \text{ mm}^3$ fused silica cell in the Cary 50 spectrometer for transmission measurement was irradiated with a 455 nm LED light source

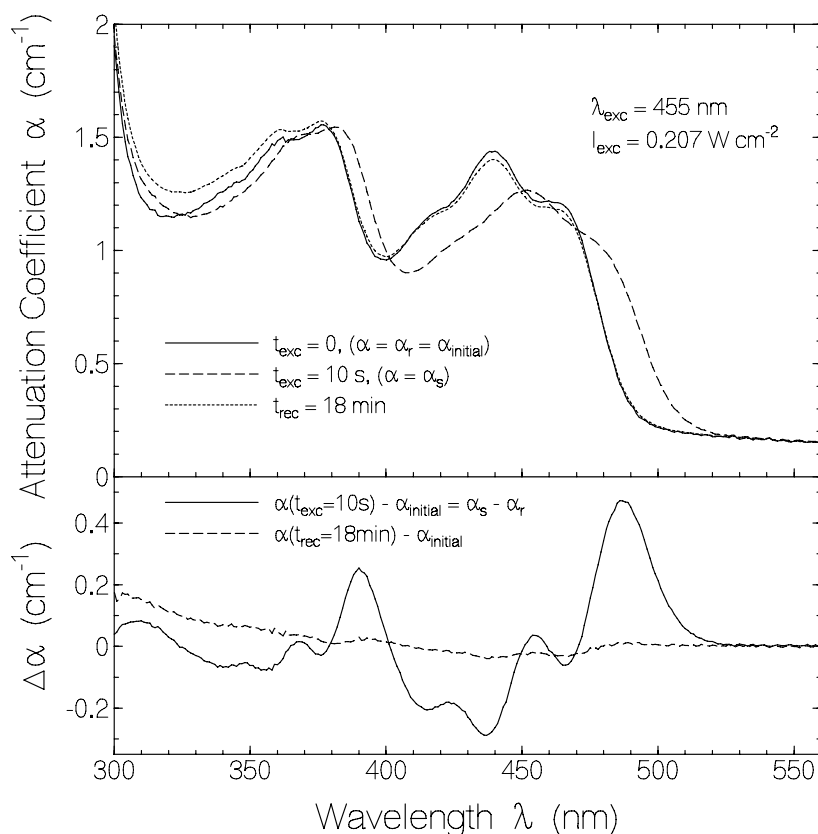


Fig. 6a. Photo-cycling behavior of LiPAC due to sample exposure at $\lambda_{\text{exc}} = 455 \text{ nm}$ with $I_{\text{exc}} = 0.207 \text{ W cm}^{-2}$ for 10 s. Top part shows attenuation coefficient spectra $\alpha(\lambda, t_{\text{exc}})$ for $t_{\text{exc}} = 0$ (solid curve, unexposed sample), $t_{\text{exc}} = 10 \text{ s}$ (dashed curve sample in signaling state), and $t_{\text{rec}} = 18 \text{ min}$ (dotted curve, sample recovered to receptor state). Bottom part shows difference attenuation coefficient spectra $\Delta\alpha(\lambda)$. The solid curve belongs to $\Delta\alpha(\lambda, t_{\text{exc}} = 10 \text{ s}) = \alpha(\lambda, t_{\text{exc}} = 10 \text{ s}) - \alpha_{\text{initial}}(\lambda) \approx \alpha_{\text{s}}(\lambda) - \alpha_{\text{r}}(\lambda)$. The dashed curve belongs to $\Delta\alpha(\lambda, t_{\text{rec}} = 18 \text{ min}) = \alpha(\lambda, t_{\text{rec}} = 18 \text{ min}) - \alpha_{\text{initial}}(\lambda)$.

transverse to the transmission detection path (exposed area $3 \times 5 \text{ mm}^2$, sample thickness along excitation path 1.5 mm, transmission detection path length 3 mm). Absorption spectra were measured before, during, and after light exposure with $I_{\text{exc}} = 0.207 \text{ W cm}^{-2}$ at $\lambda_{\text{exc}} = 455 \text{ nm}$ (Fig. 6a), and the temporal absorption kinetics at the fixed probe wavelength $\lambda_{\text{pr}} = 485 \text{ nm}$ was recorded for several excitation intensities (Fig. 6b).

At the top part of Fig. 6a the solid curve shows the attenuation coefficient spectrum of LiPAC before light exposure (LiPAC is dark-adapted, it is in the receptor state). The dashed curve belongs to LiPAC sample exposure at $\lambda_{\text{exc}} = 455 \text{ nm}$ with intensity of $I_{\text{exc}} = 0.207 \text{ W cm}^{-2}$ for a duration of $t_{\text{exc}} = 10 \text{ s}$ (LiPAC is light-adapted, it is in the signaling state). The curve shows the typical BLUF domain flavin absorption red-shift due to

photo-induced flavin – protein hydrogen bond restructuring [11, 12, 81, 82] (S_0 - S_1 absorption band red-shift $\delta\lambda_{\text{s,r}} \approx 13 \text{ nm}$). The dotted curve shows the attenuation coefficient spectrum of LiPAC measured at $t_{\text{rec}} = 18 \text{ min}$ after excitation light switch-off (total duration of light exposure $\approx 12 \text{ s}$). The flavin absorption recovered mainly from the signaling state absorption to the initial receptor state absorption after light switch-off. The amount of approximately 1.5% of free flavin was photo-degraded mainly to lumichrome [73] (see below). In the range $< 380 \text{ nm}$ some increased LiPAC absorption is observed which is thought to be mainly due to irreversible photo-conversion of non-covalently bound Fl_{ox} to Fl_{red} covalently bound to the LiPAC protein (see below). The attenuation coefficient spectra changes due to photo-excitation are displayed in the lower part of Fig. 6a. The

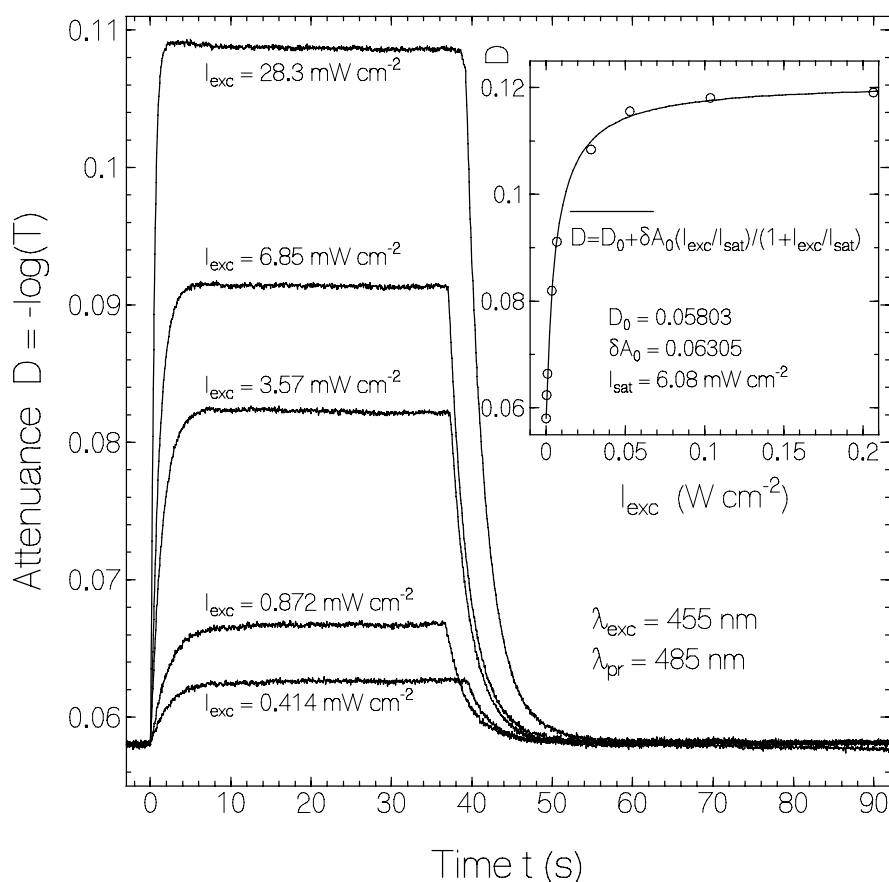


Fig. 6b. Temporal attenuation development $D(\lambda_{pr}, t)$ at $\lambda_{pr} = 485$ nm during and after sample exposure. Excitation wavelength $\lambda_{exc} = 455$ nm. Measurements carried out at room temperature (≈ 20 °C). Excitation intensities are listed at the curves. After excitation light switch-off the attenuation recovers to the dark-adapted situation with a recovery time constant of $\tau_{rec} = 2.61 \pm 0.06$ s. The inset displays the attenuation D ($\lambda_{pr} = 485$ nm, $t_{exc} = 20$ s) versus input excitation intensity I_{exc} at $\lambda_{exc} = 455$ nm. The circles correspond to experimental data. Solid curve is nonlinear regression fit of $D(I_{exc}) = D_0 + \Delta A_0(I_{exc}/I_{sat})/(1 + I_{exc}/I_{sat})$ with the fit parameters listed in the sub-figure.

solid curve shows the attenuation coefficient spectrum difference between signaling state, $\alpha_s(\lambda)$ and receptor state, $\alpha_r(\lambda)$ ($\Delta\alpha(\lambda) = \alpha(\lambda, t_{exc} = 10$ s) - $\alpha_{initial}(\lambda) = \alpha_s(\lambda) - \alpha_r(\lambda)$). The dashed curve shows the remaining absorption coefficient spectrum difference after dark recovery ($\Delta\alpha(\lambda) = \alpha(\lambda, t_{rec} = 18$ min) - $\alpha_{initial}(\lambda)$).

The attenuation development $D(\lambda_{pr}) = -\log(T(\lambda_{pr}))$ [83] at $\lambda_{pr} = 485$ nm versus time during and after light exposure at 455 nm for different input excitation light intensities I_{exc} is displayed in Fig. 6b. For the measurements the spectrophotometer Cary 50 was operated in its kinetic absorbance measurement mode at the fixed wavelength

$\lambda_{pr} = 485$ nm. In all cases the attenuation increased at light switch-on to a plateau value and remained approximately constant till light switch-off. After light switch-off the attenuation recovered to its dark-adapted value before light exposure. For the displayed curves the attenuation relaxation fits well to a single exponential decay with recovery time constant $\tau_{rec} = 2.61 \pm 0.06$ s.

The inset in Fig. 6b displays the attenuation $D(\lambda_{pr} = 485$ nm, $t_{exc} = 20$ s) versus input excitation intensity I_{exc} at $\lambda_{exc} = 455$ nm. Circles are measured data points. The solid curve is fitted to the experimental points by the relation (appendix of [11])

$$D(\lambda_{pr}, I_{exc}) = D_0(\lambda_{pr}) + \delta A(\lambda_{pr}, I_{exc}) = D_0(\lambda_{pr}) + \delta A_0(\lambda_{pr}) \frac{I_{exc} / I_{sat}}{1 + I_{exc} / I_{sat}}, \quad (2)$$

with $D_0(485 \text{ nm}) = 0.05803$, $\delta A_0(485 \text{ nm}) = 0.06305$, and $I_{sat} = 6.08 \text{ mW cm}^{-2}$.

The initial dark-adapted attenuance is given by $D_0(\lambda_{pr}) = \alpha_0(\lambda_{pr})\ell/1n(10)$ where $\alpha_0(\lambda_{pr}) = \alpha_{sca,0}(\lambda_{pr}) + \alpha_{abs,0}(\lambda_{pr})$ is the dark-adapted attenuation coefficient and ℓ is the sample length in the excitation direction ($\ell = 0.15 \text{ cm}$ in our experiments). $\delta A(\lambda_{pr}, I_{exc}) = \delta \alpha_{abs}(\lambda_{pr}, I_{exc})\ell/1n(10) = N_{Fl,s}[\sigma_s(\lambda_{pr}) - \sigma_r(\lambda_{pr})]\ell/1n(10)$ is the excitation intensity-dependent absorbance change. $N_{Fl,s}$ is the number density of flavin molecules in the signaling state, and σ_s and σ_r are the absorption cross-sections of the flavin molecules in the signaling state and the receptor state, respectively. δA_0 is given by $\delta A_0(\lambda_{pr}) = \delta \alpha_{abs,0}(\lambda_{pr})\ell/1n(10) = N_{Fl,b,0}[\sigma_s(\lambda_{pr}) - \sigma_r(\lambda_{pr})]\ell/1n(10)$ where $N_{Fl,b,0}$ is the total number density of non-covalently bound flavin ($N_{Fl,b,0} = N_{Fl,s} + N_{Fl,r}$). For $t_{exc} \gg \tau_{rec}$, $N_{Fl,s}$ is given by ([84], appendix of [11])

$$N_{Fl,s}(I_{exc}) = N_{Fl,b,0} \frac{I_{exc} / I_{sat}}{1 + I_{exc} / I_{sat}}, \quad (3)$$

where I_{sat} is the excitation saturation intensity of flavin cofactor conversion from the receptor state to the signaling state. I_{sat} is determined by the flavin absorption cross-section $\sigma_r(\lambda_{exc})$ in the receptor state at the excitation wavelength λ_{exc} , the recovery time constant τ_{rec} of the signaling state to the receptor state, and the quantum yield of signaling state formation ϕ_s according to [11, 12, 84]

$$I_{sat} = \frac{h\nu_{exc}}{\sigma_r(\lambda_{exc})\tau_{rec}\phi_s}, \quad (4a)$$

where h is the Planck constant and $\nu_{exc} = c_0/\lambda_{exc}$ is the excitation frequency (c_0 is speed of light in vacuum). The quantum yield of signaling state formation is obtained by re-expression of Eq. 4a as

$$\phi_s = \frac{h\nu_{exc}}{\sigma_r(\lambda_{exc})\tau_{rec}I_{sat}}. \quad (4b)$$

Insertion of the experimental parameters of Fig. 6b ($\tau_{rec} = 2.61 \text{ s}$, $I_{sat} \approx 0.00608 \text{ W cm}^{-2}$) with $\sigma_r(455 \text{ nm}) \approx 4.6 \times 10^{-17} \text{ cm}^2$ [73] gives $\phi_s \approx 0.60$.

The quantum yield of signaling-state formation may alternatively be determined by the more direct relation

$$\phi_s = \frac{\Delta N_s}{\Delta n_{ph,abs}}, \quad (5a)$$

where ΔN_s is the length-integrated number density of flavins converted to the signaling state, and $\Delta n_{ph,abs}$ is the number density of absorbed excitation photons. ΔN_s is given by

$$\Delta N_s = N_{Fl,b,0}\ell \frac{\delta A(\lambda_{pr})}{\delta A_{max}(\lambda_{pr})}, \quad (5b)$$

and the corresponding $\Delta n_{ph,abs}$ is given by

$$\Delta n_{ph,abs} = \frac{I_{exc}\delta t_{exc}}{h\nu_{exc}} [1 - \exp(-\alpha_{abs}(\lambda_{exc})\ell)] \approx \frac{I_{exc}\delta t_{exc}}{h\nu_{exc}} [1 - \exp(-N_{Fl,b,0}\sigma_r(\lambda_{exc})\ell)] \quad (5c)$$

where $\delta A(\lambda_{pr})$ is the absorbance change during the exposure time increment δt_{exc} at the onset of exposure, and $\delta A_{max}(\lambda_{pr})$ is the maximum absorption change due to complete conversion of flavins from the receptor state to the signaling state. Application of these equations to the curves of Fig. 6b with $N_{Fl,b,0} = 2.32 \times 10^{16} \text{ cm}^{-3}$, $\sigma_r(455 \text{ nm}) = 4.6 \times 10^{-17} \text{ cm}^2$ and $\ell = 0.15 \text{ cm}$ gives $\phi_s = 0.60 \pm 0.04$.

The transmission development $T(\lambda_{pr})$ at $\lambda_{pr} = 485 \text{ nm}$ as a function of time during and after light exposure was studied for five different sample temperatures (4 °C, 8 °C, 12 °C, 16 °C, and 20 °C). The sample was excited at 455 nm with input excitation light intensity of $I_{exc} = 0.19 \text{ W cm}^{-2}$

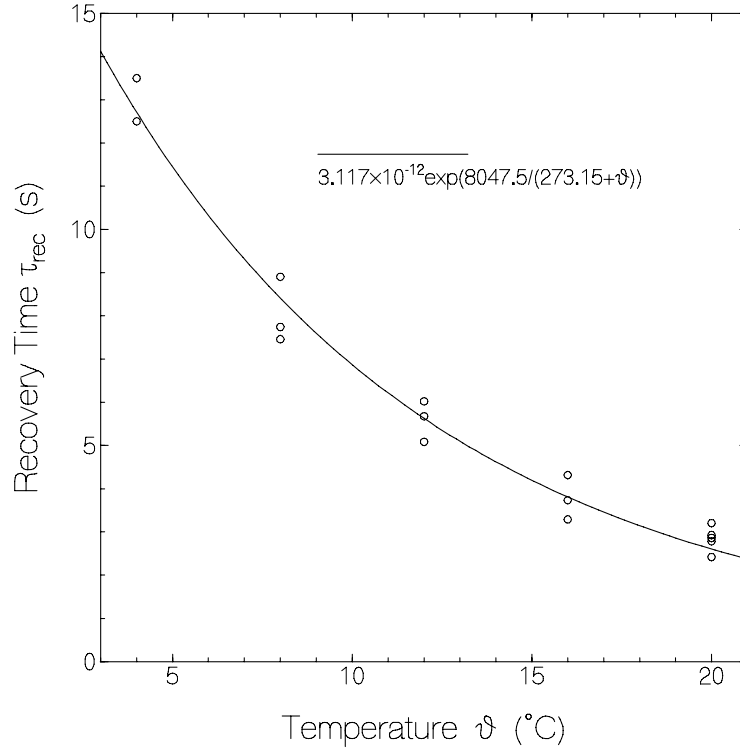


Fig. 6c. Dependence of signaling state recovery time τ_{rec} on LiPAC sample temperature ϑ . The circles correspond to experimental data. The solid curve is a nonlinear regression fit of $\tau_{\text{rec}}(\vartheta) = \tau_{\text{rec},0} \exp[\vartheta_A / (273.15^\circ\text{C} + \vartheta)]$ with barrier crossing time constant $\tau_{\text{rec},0} = 3.117 \times 10^{-12}$ s, activation temperature $\vartheta_A = 8047.5$ K, and sample temperature ϑ in $^\circ\text{C}$.

with the same excitation light source (LED 455 nm) as before (Figs. 6a and 6b). But the sample cell was put in a thermoelectric temperature controlled chamber, the probe light source was changed to a tungsten lamp with a 490 nm interference filter, and the transmitted probe light was detected with a photomultiplier tube and a LeCroy 6360 digital oscilloscope recording 10 samples per second. The oscilloscope signal traces were similar in shape to the traces shown in Fig. 6b (not shown here). They were analyzed for the determination of the signaling state recover time τ_{rec} . In Fig. 6c the determined experimental recovery times are shown by circles as a function of the applied sample temperature ϑ . The solid curve in Fig. 6c is an Arrhenius relation fit to the experimental data according to [63, 85]

with the fit parameters $\tau_{\text{rec},0} = 3.117 \times 10^{-12}$ s and $\vartheta_A = 8047.5$ K (ϑ is the temperature in $^\circ\text{C}$ and $\vartheta_K = 273.15^\circ\text{C} + \vartheta$ is the temperature in K). In Eq. 6 $\tau_{\text{rec},0}$ is the attempt time constant of barrier crossing from the ground-potential signaling state to the ground-potential receptor state, $E_A = hc_0\tilde{\nu}_A = k_B\vartheta_A$ is the ground-potential transition-state barrier-crossing activation energy, h is the Planck constant, c_0 is the vacuum light velocity, k_B is the Boltzmann constant, $\tilde{\nu}_A$ is the activation wavenumber, and ϑ_A is the activation temperature. The best fitting activation energy is $E_A = 1.11 \times 10^{-19}$ J and the corresponding activation wavenumber is $\tilde{\nu}_A = 5590$ cm^{-1} .

$$\tau_{\text{rec}}(\vartheta) = \tau_{\text{rec},0} \exp\left(\frac{\vartheta_A}{\vartheta_K}\right) = \tau_{\text{rec},0} \exp\left(\frac{E_A}{k_B\vartheta_K}\right) = \tau_{\text{rec},0} \exp\left(\frac{hc_0\tilde{\nu}_A}{k_B\vartheta_K}\right) \quad (6)$$

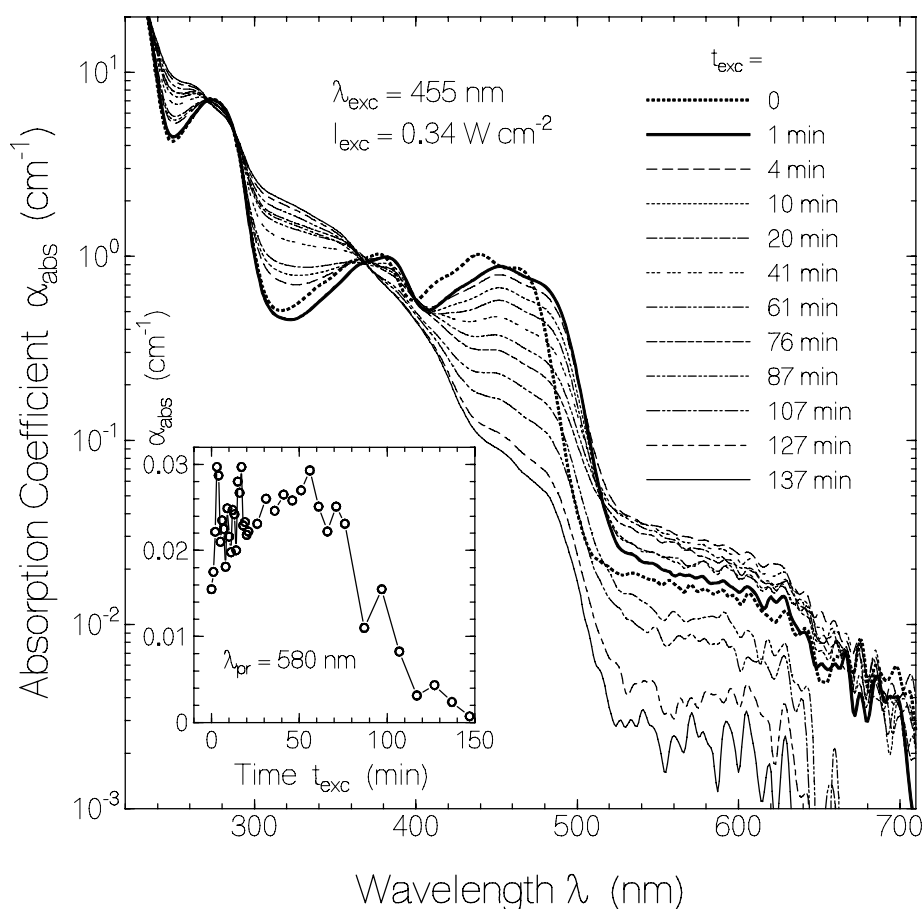


Fig. 6d. Photo-degradation of LiPAC due to photo-excitation at $\lambda_{\text{exc}} = 455 \text{ nm}$ with $I_{\text{exc}} = 0.34 \text{ W cm}^{-2}$ over a prolonged time range. The exposure times t_{exc} are listed in the legend of the curves. The inset shows the FIH absorption coefficient development at 580 nm versus exposure time.

Photo-degradation

The photo-degradation of LiPAC in the case of long-time light exposure with $I_{\text{exc}} = 0.34 \text{ W cm}^{-2}$ at $\lambda_{\text{exc}} = 455 \text{ nm}$ is displayed in Fig. 6d. Absorption coefficient spectra $\alpha_{\text{abs}}(\lambda)$ for different exposure times t_{exc} are presented (light scattering contribution is subtracted from the measured attenuation coefficient spectra). The thick dotted curve shows the absorption coefficient spectrum of LiPAC before light exposure (BLUF domain in receptor state BLUF_r). The thick solid curve belongs to $t_{\text{exc}} = 1 \text{ min}$ where the LiPAC BLUF domain is converted to the signaling state BLUF_s (red-shift of $\text{Fl}_{\text{ox}} \text{ S}_0\text{-S}_1$ absorption band). The presented $\alpha_{\text{abs}}(\lambda)$ curves with increasing exposure time show a continued photo-degradation of LiPAC in the BLUF signaling state. The Fl_{ox} component is decreased (absorption band around

450 nm). It is converted to Fl_{red} via Fl_{sq} intermediate (absorption band around 580 nm initially increases with exposure time and finally decreases). The absorption coefficient development at 580 nm versus light exposure time is depicted in the inset of Fig. 6d. The photo-degraded sample was stored for one day in the dark at 4 °C. Then it was denatured by heating up to 80 °C and cooling down (similar to heat treatment shown in Fig. 5). After centrifugation the absorption coefficient spectrum was measured. The absorption coefficient spectrum remained roughly unchanged. This observation indicates that Fl_{red} got covalently bound to the LiPAC protein in the photo-degradation process. Otherwise re-oxidation of Fl_{red} to Fl_{ox} would have occurred after protein denaturation with non-covalently bound flavin release to the solvent at aerobic conditions [86].

The quantum yield of photo-degradation ϕ_D of Fl_{ox} in the LiPAC signaling state to Fl_{red} via Fl_{sq} was calculated by application of Eqs. 5a-5c to Fig. 6d (absorption coefficient change at $\lambda = 452$ nm between curves for $t_{\text{exc}} = 4$ min and $t_{\text{exc}} = 1$ min was used). The obtained quantum yield of photo-degradation is $\phi_D = (1.1 \pm 0.1) \times 10^{-5}$.

Fluorescence lifetime behavior of LiPAC in saturated light-adapted state

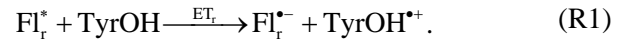
The temporal fluorescence behavior of LiPAC in the signaling state was studied by fluorescence excitation with our Ti:sapphire laser system (wavelength $\lambda_p = 400$ nm, pulse duration $\Delta t_p \approx 3$ ps) and fluorescence signal trace recording with our micro-channel-plate photomultiplier – oscilloscope detection system during transverse sample exposure at $\lambda_{\text{exc}} = 455$ nm with an intensity of $I_{\text{exc}} = 31.8 \text{ mW cm}^{-2}$ (laser fired at $t_{\text{exc}} \approx 17$ s). An obtained fluorescence trace, normalized to the maximum fluorescence signal height in the case of dark-adapted sample, is displayed by the dashed curve in the top part of Fig. 4. The fluorescence signal of non-covalently bound flavin in the signaling state is reduced to $\rho_{s,r} \approx 0.34$ of the fluorescence contribution of non-covalently bound flavin in the receptor state. The fluorescence quantum yield of light-adapted non-covalently bound flavin is $\phi_{F,Fl,b,la} = \rho_{s,r} \phi_{F,Fl,b,da} \approx 2 \times 10^{-3}$. The average lifetime of non-covalently bound flavin in the signaling state is estimated to be $\bar{\tau}_{F,Fl,b,la} = \phi_{F,Fl,b,la} \tau_{\text{rad},Fl} \approx 36$ ps using $\tau_{\text{rad},Fl} \approx \tau_{\text{rad},\text{FMN}} \approx 18$ ns [87] for the radiative flavin lifetime.

DISCUSSION

Serveral photoactivated adenylyl cyclases have been shown to stimulate the catalytic conversion of adenosine tri-phosphate (ATP) to cyclic adenosine mono-phosphate (cAMP) by blue-light exposure [6-18]. In preliminary experiments it was found that LiPAC belongs to this group of PACs with light enhanced cyclase activity (results will be given elsewhere). Comparative homology analysis of LiPAC with that of known and well characterized PAC proteins suggests the presence of important residues for the flavin binding pocket of the BLUF domain and residues important for the cyclase activity in the CHD domain (Fig. 1).

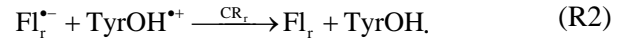
Determined parameters in this paper are collected in Table 1. The observed photo-cycling dynamics leads to a primary BLUF domain photo-cycle scheme displayed in Fig. 7a. In our approach fluorescence lifetime measurements are applied to photo-cycle parameter extraction ([51] and this work) while other groups [31, 53, 81, 82, 88, 89] use time-resolved laser pump probe experiments for this purpose.

The LiPAC BLUF domain in the dark-adapted state (receptor state) BLUF_r is exposed by blue-light (frequency ν_{exc}). Thereby, in a primary photo-cycle process, non-covalently bound fully oxidized flavin (flavin quinone, here abbreviated by Fl_r) is photo-excited to Fl_r^* . In the excited state Fl_r^* dominantly takes up an electron from an adjacent Tyr by reductive electron transfer [90] according to [9, 28, 30, 51, 53, 81, 82, 88, 89]



The time constant of the electron transfer τ_{ET_r} is given by the fast fluorescence lifetime $\tau_{F,Fl,b,da,f}$ ($\tau_{\text{ET}_r} = \tau_{F,Fl,b,da,f}$, see below).

The Fl_r^- flavin radical anion and the $\text{TyrOH}^{*\cdot}$ tyrosine radical cation recover to Fl_r and Tyr by charge recombination according to



The Fl_r^- lifetime $\tau_{\text{Fl}_r^-}$ is given by the slow fluorescence lifetime $\tau_{F,Fl,b,da,sl}$ ($\tau_{\text{Fl}_r^-} = \tau_{F,Fl,b,da,sl}$, see below). Within the lifetime $\tau_{\text{Fl}_r^-}$ of the Fl_r^- - $\text{Tyr}^{*\cdot}$ radical ion-pair there occurs restructuring of the BLUF domain - flavin binding pocket conformation and the hydrogen bond conformation due to the ion-pair electrostatic force [51]. This restructuring changes the receptor state BLUF domain BLUF_r to the signaling state BLUF domain BLUF_s (Fl_r changes to Fl_s) with quantum efficiency of signaling state formation ϕ_s . In the hydrogen bond restructuring generally an adjacent Gln residue is involved by Gln rotation [81, 82, 88, 89] or tautomerization [91, 92].

After excitation light switch-off, BLUF_s recovers to BLUF_r by thermal hydrogen bond and protein conformation restructuring to the original dark-adapted conformation according to

Table 1. Parameters of LiPAC in aqueous solution at pH 7.5 (10 mM NaH₂PO₄/ Na₂HPO₄, 10 mM NaCl).

Parameter	Value	Comments
$x_{\text{FMN,RF}}$	0.56 ± 0.1	Eq. 1
x_{FAD}	0.44 ± 0.1	Eq. 1
ϑ_{m} (°C)	54 ± 2	Fig. 5
x_{free}	0.015 ± 0.002	Fig. 3, Fig. 4
$\tau_{\text{F,free}}$ (ns)	≈ 5	Fig. 4
$\phi_{\text{F,Fl,b,da}}$	$(5.9 \pm 1) \times 10^{-3}$	Fig. 3, Fig. 4
$\tau_{\text{F,Fl,b,da,f}}$ (ps)	24.4 ± 3	$\tau_{\text{F,Fl,b,da,f}} = \tau_{\text{ET}_r}$
$x_{\text{Fl,da,f}}$	0.396 ± 0.03	Fig. 4, bottom part
$\tau_{\text{F,Fl,b,da,sl}}$ (ps)	115 ± 10	$\tau_{\text{F,Fl,b,da,sl}} = \tau_{\text{Fl}^{\bullet-}}$
$x_{\text{Fl,da,sl}}$	0.589 ± 0.03	Fig. 4, bottom part
$\delta\lambda_{\text{s,r}}$ (nm)	13 ± 1	Fig. 6a
$\rho_{\text{s,r}}$	0.34 ± 0.03	Fig. 4, top part
$\bar{\tau}_{\text{F,Fl,b,la}}$ (ps)	36 ± 4	$\phi_{\text{F,Fl,b,la}} \tau_{\text{rad,Fl}}$
τ_{rec} (s)	2.61 ± 0.06	Fig. 6b, Fig. 6c, 20 °C
I_{sat} (mW cm ⁻²)	6.08	Fig. 6b, inset
ϕ_{s}	0.6 ± 0.04	Eq. 4b
$E_{\text{A}}/(hc_0)$ (cm ⁻¹)	≈ 5590	Eq. 6, Fig. 6c
$\delta E/(hc_0)$ (cm ⁻¹)	≈ 81	Eq. 7b, Fig. 7c
ϕ_{D}	$(1.1 \pm 0.1) \times 10^{-5}$	Fig. 6d, Eq. 5a

$x_{\text{FMN,RF}}$ = mole fraction of FMN and riboflavin. x_{FAD} = mole fraction of FAD. ϑ_{m} = apparent protein melting temperature. x_{free} = mole fraction of free (released or improper bound) flavin. $\phi_{\text{F,Fl,b,da}}$ = fluorescence quantum yield of non-covalently bound flavin in the dark-adapted state. $\tau_{\text{F,Fl,b,da,f}}$ = fast fluorescence lifetime of non-covalently bound flavin in the receptor state. $\tau_{\text{F,Fl,b,da,sl}}$ = slow fluorescence lifetime of non-covalently bound flavin in the receptor state. $x_{\text{Fl,da,f}}$ = fraction of flavins with fast fluorescence decay in the dark-adapted state. $x_{\text{Fl,da,sl}}$ = fraction of flavins with slow fluorescence decay in the dark-adapted state. $\delta\lambda_{\text{s,r}}$ = red-shift of S₀-S₁ absorption band due to signaling state formation. $\rho_{\text{s,r}} = \phi_{\text{F,Fl,b,la}}/\phi_{\text{F,Fl,b,da}}$ = ratio of fluorescence quantum yields of light-adapted to dark-adapted non-covalently bound flavin. $\bar{\tau}_{\text{F,Fl,b,la}}$ = average fluorescence lifetime of non-covalently bound flavin in the signaling state. τ_{rec} = signaling state recovery time. I_{sat} = saturation intensity of signaling state formation. ϕ_{s} = quantum efficiency of signaling state formation. E_{A} = activation barrier for thermal signaling state to receptor state recovery. δE = ground-state energy level difference between tyrosine radical cation and flavin radical anion in LiPAC BLUF domain. ϕ_{D} : quantum yield of photo-degradation.



The recovery time τ_{rec} on the timescale of seconds is determined by thermal ground-potential transition-state barrier crossing.

Photo-excitation of Fl_s in the BLUF_s signaling state conformation in a secondary photo-cycle process (lower part of Figs. 7a and 7b) causes, as in the primary photo-cycle process, photo-induced reductive Tyr to excited flavin electron transfer according to

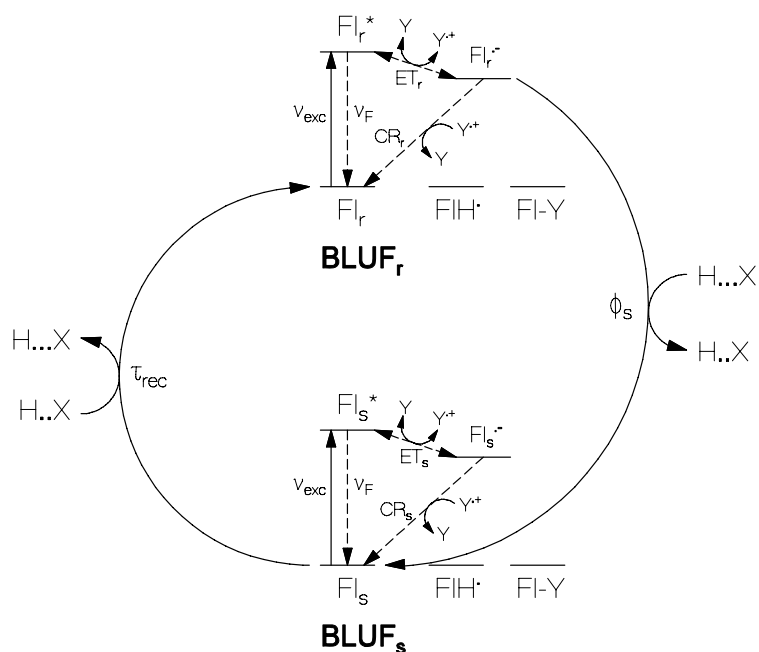


Fig. 7a. Scheme of primary photo-cycling dynamics of BLUF domain of LiPAC. For explanation see main text.

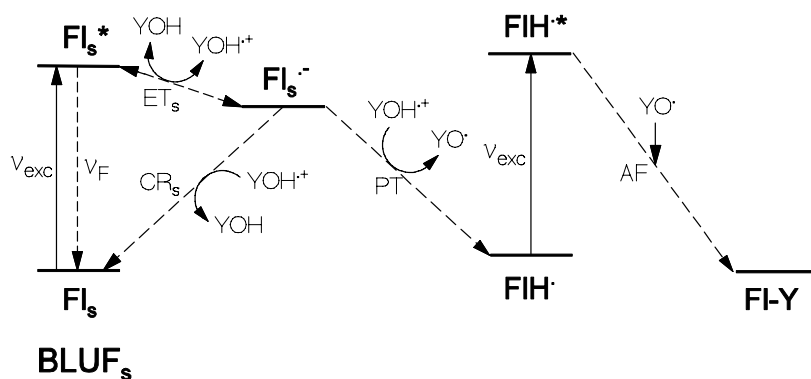
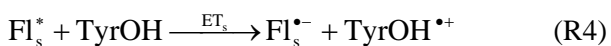


Fig. 7b. Scheme of secondary photo-dynamics of BLUF domain of LiPAC in its signaling state. ET = electron transfer, CR = charge recombination, PT = proton transfer, AF = adduct formation. For explanation see main text.



The $\text{Fl}_s^{\bullet-} + \text{TyrOH}^{\bullet+}$ radical ion pair recovers dominantly to Fl_s and Tyr according to



The electron transfer time constant $\tau_{\text{ET}_s} = \tau_{F,Fl,b,1a,f}$ is shorter than τ_{ET_r} , and the $\text{Fl}_s^{\bullet-}$ lifetime $\tau_{\text{Fl}_s^{\bullet-}} = \tau_{F,Fl,b,1a,sl}$ is shorter than $\tau_{\text{Fl}_r^{\bullet-}}$ due to a

smaller distance between flavin and tyrosine in the signaling state (electron transfer depends exponentially on distance between electron donor and electron acceptor [93]). $\text{Fl}_s^{\bullet-}$ and $\text{TyrOH}^{\bullet+}$ react with low efficiency by proton transfer to form flavin semiquinone FIH^{\bullet} and tyrosine radical TyrO^{\bullet} according to



Due to photo-excitation of FIH^{\bullet} to $\text{FIH}^{\bullet*}$, the two radicals, FIH^{\bullet} and TyrO^{\bullet} , covalently bind by

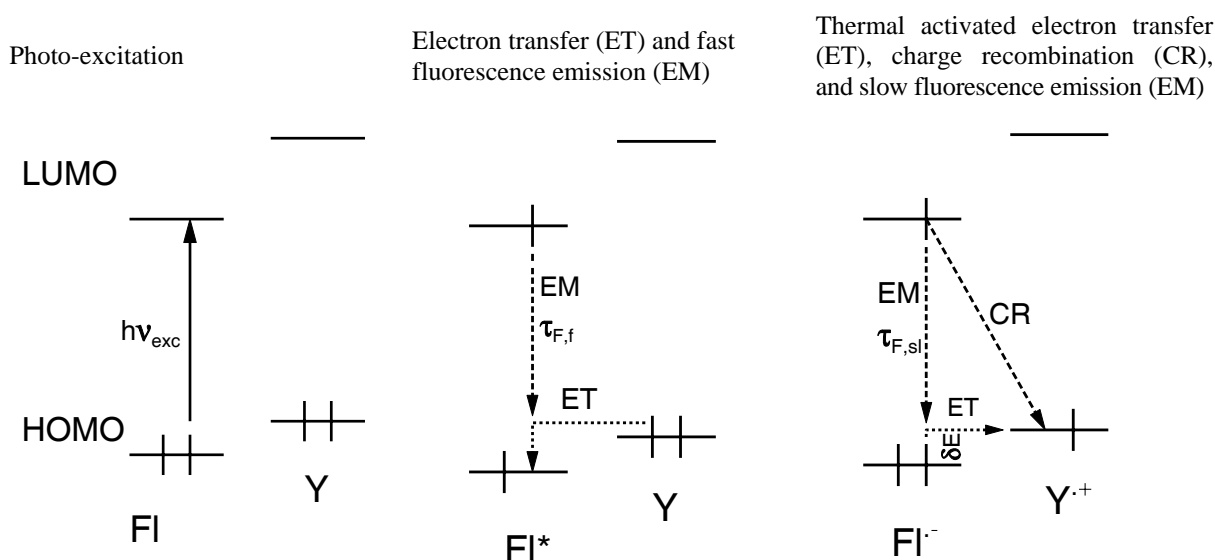


Fig. 7c. Illustration of flavin photo-excitation ($h\nu_{\text{exc}}$, left part), followed by reductive electron transfer (ET) from Tyr to Fl^* and fast fluorescence emission (EM, fluorescence lifetime $\tau_{\text{F},\text{f}}$, middle part), and subsequent charge recombination (CR) between $\text{Fl}^{\bullet-}$ (LUMO) and $\text{Tyr}^{\bullet+}$ (HOMO) and slow fluorescence emission (EM, fluorescence life-time $\tau_{\text{F},\text{s}}$, right part) both for BLUF_r and BLUF_s . Thermal activated electron transfer from $\text{Fl}^{\bullet-}$ (HOMO) to $\text{Y}^{\bullet+}$ (HOMO) (energy difference δE) enables continued fluorescence emission from Fl^* (LUMO) to Fl^* (HOMO) within the $\text{Fl}^{\bullet-}$ lifetime $\tau_{\text{Fl}^{\bullet-}}$.

adduct formation to form a reduced flavin – tyrosinyl adduct according to



whereby the reduced flavin is covalently bound to the LiPAC protein (FlH-OTyr is shortly named Fl-Tyr or Fl-Y in Fig. 7b). The quantum yield of Fl_s photo-degradation ϕ_{D} is given by the quantum yield of Fl-Tyr formation (see Fig. 7b).

The described secondary photo-excitation dynamics of BLUF_s of LiPAC is illustrated in Fig. 7b. The structural formulae of Fl_{ox} , $\text{Fl}^{\bullet-}$, FlH^{\bullet} and $\text{FlH} - \text{OTyr}$ for the situation of $\text{Fl} = \text{FMN}$ are depicted in Fig. 8. FMNH^{\bullet} is shown in the isomeric form $\text{FMNH}^{\bullet}(10\text{C}_a)$ instead of the form $\text{FMNH}^{\bullet}(4\text{C}_a)$. $\text{FMNH} - \text{OTyr}$ (named $\text{FMN} - \text{Tyr}$ in Fig. 8) is shown to be embedded in the protein via N5-O-Tyr binding. Flavoproteins containing covalently bound flavin are known in the literature [94].

The dark-adapted primary photo-cycle dynamics of BLUF domains follows generally the scheme presented in Fig. 7a. A $\text{Fl}^{\bullet-}$ to FlH^{\bullet} proton transfer

step may be involved [81, 82, 88, 89, 91, 92]. The quantitative parameters of τ_{ET} , $\tau_{\text{Fl}^{\bullet-}}$, ϕ_s , and τ_{rec} differ for different BLUF domains, and more than one recovery time constant may be observed for the recovery from the signaling state to the receptor state indicating different protein conformations.

The light-adapted secondary photo-cycle dynamics of BLUF proteins is often rather complex and different for different BLUF proteins. It may involve intermediate flavin semiquinone, reversible flavin hydroquinone, and irreversible flavin hydroquinone formation. A comparison of photo-dynamics schemes of light-adapted BLUF proteins can be found in [9]. The photo-degradation of flavins in BLUF proteins to reduced flavin protein adducts is discussed here for the first time. The irreversible flavin hydroquinone formation observed for BlrB from *Rhodobacter sphaeroides* [28], nPAC (NgPAC1) from *Naegleria gruberi* [9], Slr1694 from *Synechocystis* sp. PCC6803 [36], and BlrP1 from *Klebsiella pneumonia* [30] was not studied in detail. The irreversible flavin hydroquinone formation in these cases may

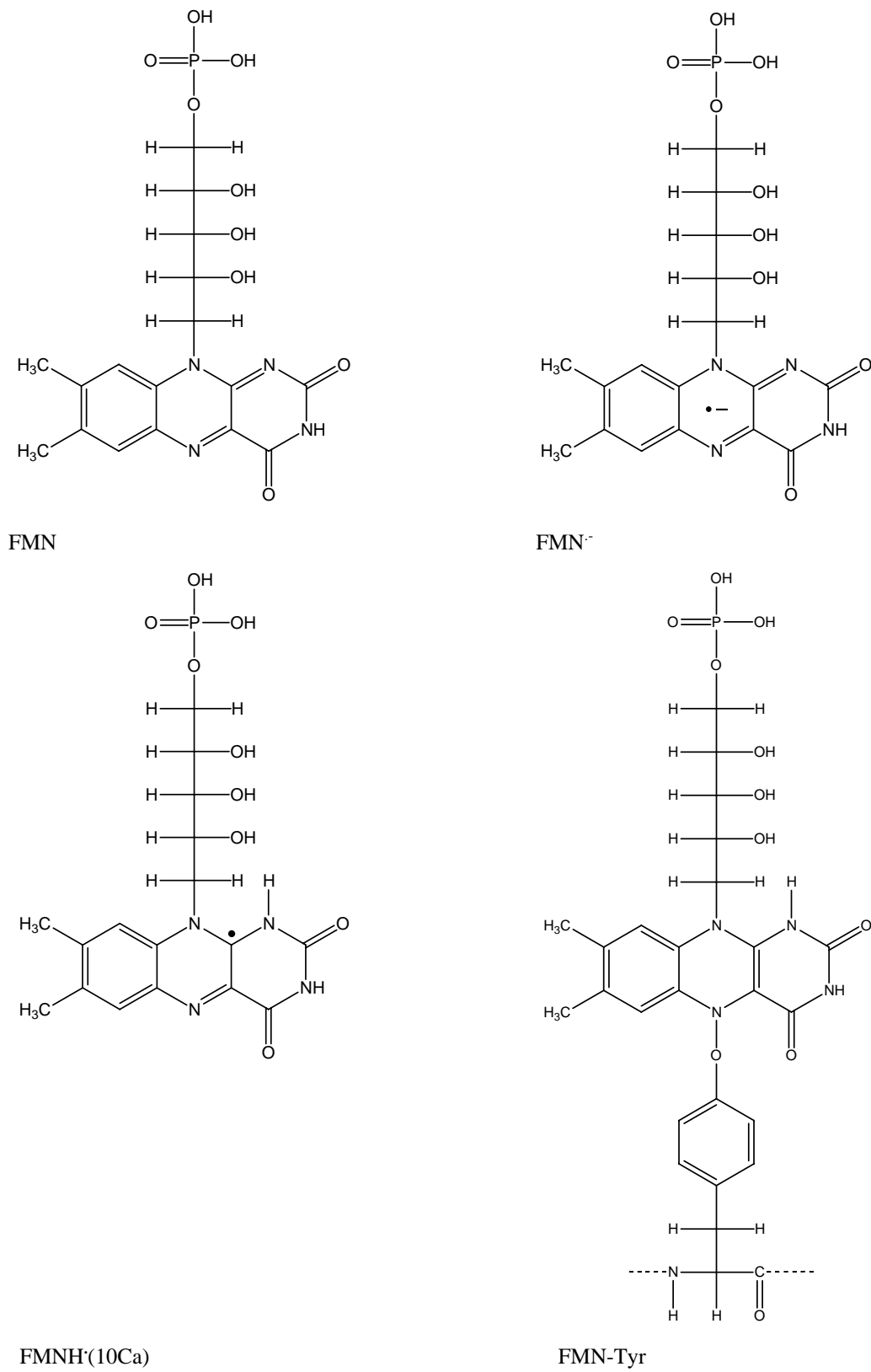


Fig. 8. Structural formulae of FMN, FMN^{•-}, FMNH[•](10Ca), and FMN-tyrosinyl adduct embedded in protein.

have been – like in this paper – due to a covalent flavin hydroquinone protein-adduct binding.

The photo-induced electron transfer and charge recombination in BLUF_r (primary excitation) and BLUF_s (secondary excitation) is illustrated in Fig. 7c [51]. The HOMO (highest occupied molecular orbital) levels and LUMO (lowest unoccupied molecular orbital) levels of flavin Fl and adjacent tyrosine Y are displayed. Photo-excitation of flavin transfers one electron from double occupied Fl(HOMO) to unoccupied Fl(LUMO) (left part of Fig. 7c) giving single occupied Fl*(HOMO) and single occupied Fl*(LUMO) (middle part of Fig. 7c). Now, in the reductive electron transfer process, an electron from double occupied Y(HOMO) transfers to the free position of Fl*(HOMO) (middle part of Fig. 7c). This transfer with the time constant τ_{ET} limits the fluorescence emission from Fl*(LUMO) to Fl*(HOMO). Therefore τ_{ET} determines the fast

fluorescence time constant $\tau_{F,Fl,b,f}$, i.e. $\tau_{F,Fl,b,f} = \tau_{ET}$. A thermal equilibrium between Fl*(HOMO) – Y(HOMO) and Fl^{•-}(HOMO) – Y^{•+}(HOMO) is established by the energy level difference δE between Fl^{•-}(HOMO) and Y^{•+}(HOMO) (right part of Fig. 7c). The presence of single-occupied Fl*(HOMO) molecules after electron transfer equilibration allows continued Fl*(LUMO) → Fl*(HOMO) fluorescence emission with fluorescence lifetime $\tau_{F,Fl,b,sl} = \tau_{Fl^{•-}}$. The thermal equilibration between Fl_i* and Fl_i^{•-} (i = r,s) is indicated by double arrows in Fig. 7a and Fig. 7b. The double fluorescence emission situation described here is similar to the prompt and delayed fluorescence emission situation of singlet – triplet intersystem crossing in molecules [95].

The non-covalently bound flavin fluorescence is given by

$$S_{F,Fl,b}(t) = S_{F,Fl,0} \left[x_{b,f} \exp(-t/\tau_{F,Fl,b,f}) + x_{b,sl} \exp(-t/\tau_{F,Fl,b,sl}) \right] \quad (7a)$$

With $x_{b,f} + x_{b,sl} = 1$ and [96]

$$x_{b,sl} = \frac{\exp\left(-\frac{\delta E}{k_B \mathcal{G}}\right)}{1 + \exp\left(-\frac{\delta E}{k_B \mathcal{G}}\right)} \quad (7b)$$

In our fluorescence lifetime measurements on dark-adapted LiPAC we found (lower part of Fig. 4) $x_{b,f} = 0.402$ and $x_{b,sl} = 0.598$. Insertion of $x_{b,sl}$ in Eq. 7b and solving for δE gives $\delta E = -\ln[x_{b,sl}/(1-x_{b,sl})]k_B \mathcal{G} = 1.61 \times 10^{-21} \text{ J} = hc_0 \times 81 \text{ cm}^{-1}$.

CONCLUSIONS

The photoactivated adenylyl cyclase LiPAC from the spirochete bacterium *Leptonema illini* strain 3055[†] was synthesized and characterized by optical spectroscopic methods. The BLUF domain photo-cycling efficiency of receptor state to signaling state conversion was found to be reasonably high (quantum yield of signaling state formation $\approx 60\%$), and the thermal recovery of the

signaling state to the receptor state was found to be rather fast (recovery time $\approx 2.6 \text{ s}$ at $20 \text{ }^\circ\text{C}$). The thermal stability of LiPAC turned out to be high (apparent protein melting temperature of $\approx 54 \text{ }^\circ\text{C}$) allowing convenient stable experimentation at room temperature with this photoactivated cyclase.

In fresh-prepared dark-adapted LiPAC, part of the flavin cofactor was present in reduced form covalently bound to the protein. Blue-light photo-excitation of LiPAC caused low-efficient irreversible photo-degradation of the non-covalently bound Fl_{ox} to covalently-bound reduced flavin Fl_{red} (quantum yield of photo-degradation $\approx 1.1 \times 10^{-5}$).

ACKNOWLEDGEMENTS

DST-SERB, Govt. of India is acknowledged for financial support of the project (SB/EMEQ-188/2013). A P. thanks Prof. F. J. Gießibl, University of Regensburg, for his kind hospitality. The authors thank Prof. P. Hegemann, Humboldt University to Berlin, for continued support.

CONFLICT OF INTEREST STATEMENT

We certify that there is no conflict of interest with any financial organization regarding the material discussed in the manuscript.

REFERENCES

1. Tripathy, D. N. and Hanson, L. E. 1972, *Am. J. Vet. Res.*, 33, 1723.
2. Woo, T. H., Patel, B. K. C., Cinco, M., Smythe, L. D., Symonds, M. L., Norris, M. A. and Dohnt, M. F. 1998, *Anal. Biochem.*, 259, 112.
3. Hovind-Hougen, K. 1979, *Int. J. Systematic Bacteriology*, 29, 245.
4. Hovind-Hougen, K. 1983, *International J. Syst. Bacteriol.*, 33, 438.
5. Huntemann, M., Stackebrandt, E., Held, B., Nolan, M., Lucas, S., Hammon, N., Deshpande, S., Cheng, J.-F., Tapia, R., Tapia, L. A., Pitluck, S., Liolios, K., Pagani, I., Ivanova, N., Mavromatis, K., Mikhailova, N., Pati, A., Chen, A., Palaniappan, K., Land, M., Rohde, M., Gronow, S., Göker, M., Detter, J. C., Bristow, J., Eisen, J. A., Markowitz, V., Woyke, T., Hugenholtz, P., Kyrpides, N. C., Klenk, H.-P. and Lapidus, A. 2013, *Standards in Genomic Sciences*, 8, 177.
6. Iseki, M., Matsunaga, S., Murakami, A., Ohno, K., Shiga, K., Yoshida, K., Sugai, M., Takahashi, T., Hori, T. and Watanabe, M. 2002, *Nature*, 415, 1047.
7. Ryu, M.-H., Moskvina, O. V., Siltberg-Lieberle, J. and Gomelsky, M. 2010, *J. Biol. Chem.*, 285, 41501.
8. Stierl, M., Stumpf, P., Udvari, D., Gueta, R., Hagedorn, R., Losi, A., Gärtner, W., Petereit, L., Efetova, M., Schwarzel, M., Oertner, T. G., Nagl, G. and Hegemann, P. 2011, *J. Biol. Chem.*, 286, 1181.
9. Penzkofer, A., Stierl, M., Hegemann, P. and Kateriya, S. 2011, *Chem. Phys.*, 387, 25.
10. Penzkofer, A., Tanwar, M., Veetil, S. K., Kateriya, S., Stierl, M. and Hegemann, P. 2013, *Chem. Phys.*, 12, 6.
11. Penzkofer, A., Stierl, M., Mathes, T. and Hegemann, P. 2014, *J. Photochem. Photobiol. B: Biol.*, 140, 182.
12. Penzkofer, A., Tanwar, M., Veetil, S. K., Kateriya, S., Stierl, M. and Hegemann, P. 2014, *J. Photochem. Photobiol. A: Chem.*, 287, 19.
13. Tanwar, M., Stierl, M., Veetil, S. K., Penzkofer, A., Hegemann, P. and Kateriya, S. 2014, *J. Proteins Proteomics*, 5, 35.
14. Ntefidou, M. M., Iseki, M., Watanabe, M., Lebert, M. and Häder, D.-P. 2003, *Plant Physiol.*, 133, 1517.
15. Ntefidou, M. M., Lüdtke, T., Ahmad, M. and Häder, D.-P. 2006, *Photochem. Photobiol.*, 82, 1601.
16. Schröder-Lang, S., Schwärzel, M., Seifert, R., Strünker, T., Kateriya, S., Looser, J., Watanabe, M., Kaupp, U. B., Hegemann, P. and Nagel, G. 2007, *Nature Meth.*, 4, 39.
17. Nagahama, T., Suzuki, T., Yoshikawa, S. and Iseki, M. 2007, *Neurosci. Res.*, 59, 81.
18. Bucher, D. and Buchner, E. 2009, *J. Neurogen.*, 23, 220.
19. Linder, J. U. and Schultz, J. E. 2003, *Cellular Signalling*, 15, 11081.
20. Hofer, A. M. and Lefkimmatis, K. 2007, *Physiology*, 22, 320.
21. Miesenböck, G. 2011, *Annu. Rev. Cell Dev. Dev.*, 27, 731.
22. Christie, J. M., Gawthorne, J., Young, G., Fraser, N. J. and Roe, A. J. 2012, *Mol. Plant*, 5, 533.
23. Weissenberger, S., Schultheis, C., Liewald, J. F., Erbguth, K., Nagel, G. and Gottschalk, A. 2011, *J. Neurochem.*, 116, 616.
24. Hong, K. P., Spitzer, N. C. and Nicol, X. 2011, *BMC Res. Notes*, 4, 241.
25. Stierl, M., Penzkofer, A., Kennis, J. T. M., Hegemann, P. and Mathes, T. 2014, *Biochem.*, 53, 5121.
26. Yasukawa, H., Sagto, A., Kita, A., Kodaira, K., Iseki, M., Takahashi, T., Shibusa, M., Watanabe, M. and Yagita, K. 2013, *J. Gen. Appl. Microbiol.*, 59, 361.
27. Gomelsky, M. and Klug, G. 2002, *Trends in Biochem. Sci.*, 27, 497.
28. Zirak, P., Penzkofer, A., Schiereis, T., Hegemann, P., Jung, A. and Schlichting, I. 2006, *J. Photochem. Photobiol. B: Biol.*, 83, 180.
29. Laan, W., Gauden, M., Yermenko, S., van Grondelle, R., Kennis, J. T. M. and Hellingwerf, K. J. 2006, *Biochem.*, 45, 51.
30. Tyagi, A., Penzkofer, A., Griese, J., Schlichting, I., Kirienko, N. V. and Gomelsky, M. 2008, *Chem. Phys.*, 354, 130.

31. Gauden, M., Grinstead, J. S., Laan, W., van Stokkum, I. H. M., Avila-Perez, M., Toh, K. C., Boelens, R., Captain, R., van Grondelle, R., Hellingwerf, K. J. and Kennis, J. T. M. 2007, *Biochem.*, 46, 7405.
32. Jung, A., Domratcheva, T., Tarutina, M., Wu, Q., Ko, W.-H., Shoeman, R. L., Gomelsky, M., Gardener, K. H. and Schlichting, I. 2005, *PNAS*, 102, 12350.
33. Okajima, K., Fukushima, Y., Suzuki, H., Kita, A., Ochiai, Y., Katayama, M., Shibata, Y., Miki, K., Noguchi, T., Itoh, S. and Ikeuchi, M. 2006, *J. Mol. Biol.*, 363, 10.
34. Kita, A., Okajima, K., Morimoto, Y., Ikeuchi, M. and Miki, K. 2005, *J. Mol. Biol.*, 349, 1.
35. Hasegawa, K., Masuda, S. and Ono, T. 2005, *Plant Cell Physiol.*, 46, 136.
36. Zirak, P., Penzkofer, A., Lehmpfuhl, C., Mathes, T. and Hegemann, P. 2007, *J. Photochem. Photobiol. B: Biol.*, 86, 22.
37. Yuan, H., Anderson, S., Masuda, S., Dragnea, V., Moffat, K. and Bauer, C. 2006, *Biochem.*, 45, 12687.
38. Barends, T. R. M., Hartmann, E., Griese, J., Beitlich, T., Kirienko, N. V., Ryjenkov, D. A., Reinstein, J., Shoeman, R. L., Gomelsky, M. and Schlichting, I. 2009, *Nature*, 459, 1015.
39. Kanazawa, T., Ren, S., Maekawa, M., Hasegawa, K., Arisaka, F., Hyodo, M., Hayakawa, Y., Ohta, H. and Masuda, S. 2010, *Biochem.*, 49, 10647.
40. Zirak, P., Penzkofer, A., Schiereis, T., Hegemann, P., Jung, A. and Schlichting, I. 2005, *Chem. Phys.*, 315, 142.
41. Stelling, A., Ronayne, K. I., Nappa, J., Tonge, P. J. and Meech, S. R. 2007, *J. Am. Chem. Soc.*, 129, 15556.
42. Golic, A., Vanechoutte, M., Nemeč, A., Viale, A. M., Actis, L. A. and Mussi, M. A. 2013, *PLoS One*, 8, e55059.
43. Bitrian, M., González, R. H., Paris, G., Hellingwerf, K. J. and Nudel, C. B. 2013, *Microbiology*, 159, 1828.
44. Zoltowski, B. D. and Gardner, K. H. 2011, *Biochem.*, 50, 4.
45. Losi, A. 2007, *Photochem. Photobiol.*, 83, 1283.
46. Losi, A. and Gärtner, W. 2011, *Photochem. Photobiol.*, 87, 491.
47. Masuda, S. 2013, *Plant Cell Physiol.*, 54, 171.
48. Wu, Q., Ko, W. H. and Gardner, K. H. 2008, *Biochem.*, 47, 10271.
49. Okajima, K., Yoshihara, S., Fukushima, Y., Geng, X., Katayama, M., Higashi, S., Watanabe, M., Sato, S., Tabata, S., Shibata, Y., Itoh, S. and Ikeuchi, M. 2005, *J. Biochem.*, 137, 741.
50. Masuda, S. and Bauer, C. E. 2002, *Cell*, 110, 613.
51. Zirak, P., Penzkofer, A., Hegemann, P. and Mathes, T. 2007, *Chem. Phys.*, 335, 15.
52. Jung, A., Reinstein, J., Domratcheva, T., Shoeman, R. L. and Schlichting, I. 2006, *J. Mol. Biol.*, 362, 717.
53. Toh, K. C., van Stokkum, I. H. M., Hendriks, J., Alexandre, M. T. A., Arents, J. C., Perez, M. A., van Grondelle, R., Hellingwerf, J. K. and Kennis, J. T. M. 2008, *Biophys. J.*, 95, 312.
54. Anderson, S., Dragnea, V., Masuda, S., Ybe, J., Moffat, K. and Bauer, C. 2005, *Biochem.*, 44, 7998.
55. Braatsch, S., Gomelsky, M., Kuphal, S. and Klug, G. 2002, *Mol. Microbiol.*, 45, 827.
56. Wu, Q. and Gardner, K. H. 2009, *Biochem.*, 48, 2620.
57. Tschowri, N., Busse, S. and Hengge, R. 2009, *Genes Dev.*, 23, 522.
58. Förster, Th. 1951, *Fluoreszenz organischer Verbindungen*. Vandenhoeck und Ruprecht, Göttingen, Germany.
59. Holzer, W., Pichlmaier, M., Penzkofer, A., Bradley, D. D. C. and Blau, W. J. 1999, *Chem. Phys.*, 246, 445.
60. Penzkofer, A. 2012, *Chem. Phys.*, 400, 142.
61. Sens, R. 1984, *Strahlungslose Desaktivierung in Xanthen, Oxazin und Carbazinfarbstoffen*, Dissertation Universität-Gesamthochschule Siegen, Germany.
62. Birkmann, C., Penzkofer, A. and Tsuboi, T. 2003, *Appl. Phys. B*, 77, 625.
63. Penzkofer, A., Stierl, M., Hegemann, P. and Kateriya, S. 2011, *J. Photochem. Photobiol. A: Chem.*, 225, 42.
64. Thompson, J. D., Gibson, T. J., Plewniak, F., Jeanmougin, F. and Higgins, D. G. 1997, *Nucleic Acids Res.*, 25, 4876.

65. Chenna, R., Sugawara, H., Koike, T., Lopez, R., Gibson, T. J., Higgins, D. G. and Thompson, J. D. 2003, *Nucleic Acids Res.*, 31, 3497.
66. Edgar, R. C. 2004, *Nucleic Acids Res.*, 32, 1792.
67. Penzkofer, A., Shirdel, J., Zirak, P., Breitreuz, H. and Wolf, E. 2007, *Chem. Phys.*, 342, 55.
68. Jagger, J. 1967, *Introduction to Research in Ultraviolet Photobiology*, Prentice Hall, Englewood Cliffs, NJ, USA, p. 53.
69. Oster, G. 1955, *Physical Techniques in Biological Research*, Vol. 1: Optical Techniques, G. Oster and A. W. Pollister (Eds.), Academic Press, New York, pp. 51.
70. Müller, F. (Ed.) 1991, *Chemistry and Biochemistry of Flavoenzymes*, CRC Press, Boca Raton, FL, USA, Volume 1.
71. Song, S.-H., Dick, B. and Penzkofer, A. 2007, *Chem. Phys.*, 332, 55.
72. Song, S.-H., Dick, B., Penzkofer, A. and Hegemann, P. 2007, *Photochem. Photobiol. B: Biol.*, 87, 37.
73. Holzer, W., Shirdel, J., Zirak, P., Penzkofer, A., Hegemann, P., Deutzmann, R. and Hochmuth, E. 2005, *Chem. Phys.*, 308, 69.
74. Lindsey, J. *PhotochemCAD Spectra by Category*, <http://omlc.org/spectra/PhotochemCAD/index.html>
75. Penzkofer, A., Luck, M., Mathes, T. and Hegemann, P. 2014, *Photochem. Photobiol.*, 90, 773.
76. Vavilov, S. I. 1927, *Z. Phys.*, 42, 311.
77. Lewis, G. N. and Kasha, M. 1944, *J. Am. Chem. Soc.*, 66, 2100.
78. Islam, S. D. M., Susdorf, T., Penzkofer, A. and Hegemann, P. 2003, *Chem. Phys.*, 295, 139.
79. Drössler, P., Holzer, W., Penzkofer, A. and Hegemann, P. 2002, *Chem. Phys.*, 282, 429.
80. Laan, W., Bednarz, T., Heberle, J. and Hellingwerf, K. J. 2004, *Photochem. Photobiol. Sci.*, 3, 1011.
81. Gauden, M., van Stokkum, I. H. M., Key, J. M., Lührs, D. C., van Grondelle, R., Hegemann, P. and Kennis, J. T. M. 2006, *PNAS*, 103, 10895.
82. Bonetti, C., Mathes, T., van Stokkum, I. H. M., Mullen, K. M., Groot, M.-L., van Grondelle, R., Hegemann, P. and Kennis, J. T. M. 2008, *Biophys. J.*, 95, 4790.
83. Dixon, H. B. F. 1992, *Biochem. Education*, 20, 108.
84. Hercher, M. 1967, *Appl. Opt.*, 6, 947.
85. Fleming, G. R. 1986, *Chemical Applications of Ultrafast Spectroscopy*, Oxford University Press, New York.
86. Song, S.-H., Dick, B. and Penzkofer, A. 2007, *Chem. Phys.*, 332, 55.
87. Holzer, W., Penzkofer, A., Fuhrmann, M. and Hegemann, P. 2002, *Photochem. Photobiol.*, 75, 479.
88. Fujisawa, T., Takeuchi, S., Masuda, S., Tahara, T. 2014, *J. Phys. Chem. B*, 118, 14761.
89. Mathes, T., van Stokkum, I. H. M., Bonetti, C., Hegemann, P. and Kennis, J. T. M. 2011, *J. Phys. Chem. B*, 115, 7963.
90. Valeur, B. 2001, *Molecular Fluorescence, Principles and Applications*, Wiley-VCH, Weinheim, Germany.
91. Sadeghian, K., Bocola, M. and Schütz, M. 2008, *J. Am. Chem. Soc.*, 130, 12501.
92. Domratcheva, T., Grigorenko, B. L., Schlichting, I. and Nemukhin, A. V. 2008, *Biophys. J.*, 94, 3872.
93. Moser, C. C., Keske, J. M., Warncke, K., Farid, R. S. and Dutton, P. L. 1992, *Nature*, 355, 796.
94. Heuts, D. P. H. M., Scrutton, N. S., McIntire, W. S. and Fraaije, M. W. 2009, *FEBS Journal*, 276, 3405.
95. Penzkofer, A., Tyagi, A., Slyusareva, E. and Sizykh, A. 2010, *Chem. Phys.*, 378, 58.
96. Bäumlér, W. and Penzkofer, A. 1988, *Chem. Phys. Lett.*, 150, 315.
97. Garnier, J., Gibrat, J. F. and Robson, B. 1996, *Meth. Enzymol.*, 266, 540.